MSc Thesis in Cold Climate Engineering

The Effects of Meltwater, Refreezing and Modelled Grain Size on Snow Albedo: Gaining Knowledge from Observations at Weather Stations and Numerical Modelling

Dominic Saunderson

s161551 | 603889

Supervisors

Thomas Ingeman-Nielsen

Miina A. Rautiainen

Advisor

Baptiste R.M. Vandecrux

Submitted

2nd June 2018

Preface

This thesis has been prepared as the final competence for the MSc Cold Climate Engineering degree, completed at the Technical University of Denmark (DTU), Copenhagen, Denmark, and Aalto University, Espoo, Finland. The thesis was jointly supervised by Prof. Thomas Ingeman-Nielsen (DTU) and Prof. Miina A. Rautiainen (Aalto); Baptiste Vandecrux (DTU) acted as an advisor.

The focus of the thesis is the parameterisation of snow albedo, using data from the PROMICE network of weather stations across the Greenland Ice Sheet (Ahlstrøm et al., 2008) and output from a firn evolution model (Vandecrux et al., in review). This document represents 5 months of work, from 2nd January 2018 to 2nd June 2018, corresponding to 30 ECTS. All work is my own, with expert guidance from the supervisory team to whom I would like to extend my sincerest gratitude for their support.

Abstract

The extent to which snow and ice surfaces undergo melt is mainly dictated by their absorption of shortwave radiation, and thus the surface albedo is a critical parameter for accurately modelling the surface energy balance and mass balance of the Greenland Ice Sheet (GrIS). Multiple variables affect the surface albedo, including the atmospheric conditions, the solar zenith angle (SZA), and the snowpack's characteristics.

This thesis uses output from a firn evolution model (Vandecrux et al., in review) to explain 8 years of albedo observations from the Kangerlussuaq Upper (KAN_U) automatic weather station (PROMICE; Ahlstrøm et al., 2008). A parameterised model is developed that differentiates between three snow conditions (aged, refrozen, and wet), and uses four variables as input: the SZA; the Sky-Air Temperature Ratio (SATR); the Liquid Water Content (LWC); and the modelled grain size.

When compared to the observed albedo at KAN_U, the model could explain more than 60% of the observed albedo variation for 2009, 2010, 2011 and 2015, but this fell below 30% for 2014. So far, no reasons for these differences have been uncovered. Each of the three snow conditions performed approximately equally well, and only the lightly cloudy skies were seen to be identifiable worse compared to any other cloud cover. The model was also largely consistent between months, with the exception of October, when the poor fit is attributed to the very short days and consistently high SZAs.

An immediate priority is to test the model against albedo observations from other PROMICE datasets. It is unclear how applicable the model will be to other locations, because it explicitly replicates a rising albedo from the early morning to noon. This was consistently seen in the observational data at KAN_U but contradicts the accepted theory. However, it is possible that the approach used by this parameterisation could be easily modified and tuned to alternative locations.

Contents

List of Figures

List of Tables

1 Introduction

1.1 Motivation

The Greenland Ice Sheet (GrIS) covers ~1.7 million square kilometres, and contains enough ice to raise sea levels by ~7m (Gregory et al., 2004) making it imperative to understand how the GrIS will respond to rising surface air temperatures.

Since the early 1990's, the GrIS has been losing ice mass (Ewert et al., 2012; Sasgen et al., 2012; Shepherd et al., 2012), and very likely at an increasing rate (Vaughan et al., 2013). Across the entire GrIS, the cause of these losses is split almost equally between dynamic ice movements and melt from the surface (van den Broeke et al., 2009). Understanding the radiative energy exchanges at the surface is therefore of the utmost importance, particularly as the magnitude (Ngheim et al., 2012) and frequency (Hanna et al., 2011) of melt events appear to be increasing.

Alongside fieldwork and remote sensing, many efforts to improve our understanding of the GrIS come from the climate modelling community, using state-of-the-art models at both the regional and global scales. However, there is no consensus on how to include albedo in such large-scale models (Gardner & Sharp, 2010; Kuipers Munneke et al., 2011), and the schemes used vary in complexity and applicability. For the Polar Regions, which are dominated by highly reflective snow and ice surfaces, getting the albedo correct is crucial, particularly because of the self-perpetuating surface-albedo feedback (Sellers, 1969; Hall, 2004; Box et al., 2012; section 2.1.2).

1.2 Research Novelty

As outlined in Chapter 2.3, many previous attempts at modelling snow albedo exist, with varying degrees of complexity and applicability. However, this thesis differs from these as it aims to create a novel parameterisation, based on data from PROMICE weather station datasets (Ahlstrøm et al., 2008) and a firn evolution model (Vandecrux et al., in review).

These datasets provide ~8 years of hourly weather and firn data that have never been used as a basis for parameterising albedo before. It is envisioned that such data will provide a unique insight into how the parameters can be used to replicate the albedo variation seen in field measurements. Finally, it is hoped that such a scheme may be seen as an upgrade on existing approaches and deemed successful enough to be considered in future ice sheet models.

1.3 Aims & Objectives

The overarching aim of this thesis is to create a novel parameterisation for snow albedo. In order to achieve this aim, the following objectives have been defined:

- To carry out a literature review into the physical controls on snow albedo;
- To identify previous snow albedo parameterisations and understand the benefits and drawbacks of such approaches;
- To quantify the relationship between albedo and PROMICE weather station data;
- To quantify the relationship between albedo and output from a firn evolution model;
- To formulate a novel parameterisation for snow albedo;
- To evaluate the success of the new parameterisation.

1.4 Thesis Contents

Chapter 2 explains the scientific background for snow albedo, identifying the parameters that can be used as a physical basis for the parameterisation, and presenting examples of previous parameterisations.

Chapter 3 introduces the PROMICE monitoring network and the firn model, and explains the parameters available from these datasets. Chapter 4 documents the process of identifying relationships between the identified parameters and albedo, and presents the parameterisation. Chapter 5 compares the parameterisation to the observed albedo dataset. Chapter 6 discusses the success of the scheme and expands on some important decisions. Finally, Chapter 7 concludes the thesis, reiterating key points and the applicability of the scheme.

2 Scientific Background

This chapter explains the scientific background for the thesis: the term albedo is defined; its importance for the Arctic is outlined; known controls on snow albedo are explained; and examples of previous parameterisations are presented.

2.1 Albedo

2.1.1 Definition

Albedo (α) is a measure of a surface's reflectivity, and is defined as the ratio of outgoing to incoming radiation (Warren, 1982). There are many related reflectance definitions in the literature, such as the Bidirectional Reflectance Distribution Function (BRDF); the Directional-Hemispherical Reflectance (DHR); and the Hemispherical-Directional Reflectance Factor (HDRF). However, albedo differs to these as it is concerned with the incoming and outgoing radiation across *all* incidence and reflection angles (Figure 1). Albedo is technically referred to as the Bihemispherical Reflectance (BHR).

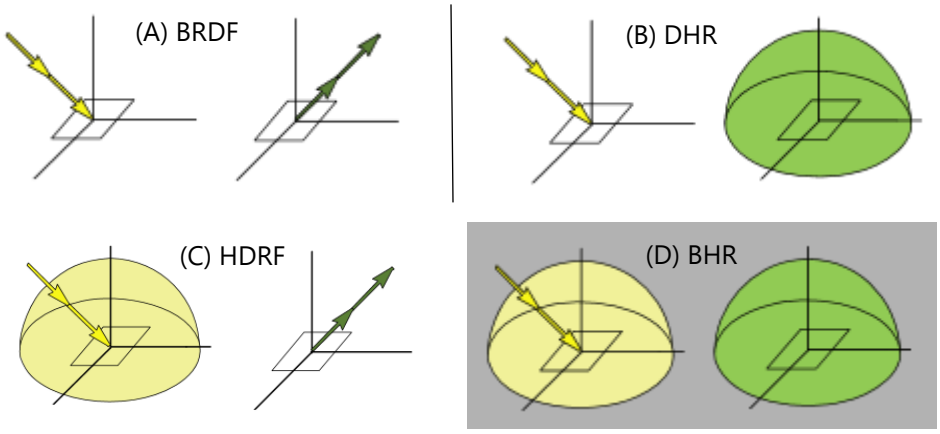

Figure 1: Schematic of selected reflectance definitions
a) BRDF – The scattering of an incident beam into another direction
b) DHR – The reflected flux of an incident beam from a single direction, across the entire hemisphere
c) HDRF - The reflected flux from the entire hemisphere, into a single direction
d) BHR/Albedo – The reflected flux from the entire hemisphere, across the entire hemisphere
Source: Schaepman-Strub et al. (2006)

Albedo can be separated into a diffuse component (*white-sky* albedo), and a direct component (*black-sky* albedo; equivalent to the DHR). Combined, the black- and white-sky albedo are known as the blue-sky albedo, with values ranging from total absorption (α=0) to total reflection (α=1).

Albedo may be formally written as:

$$\alpha = \frac{\int_{\lambda_1}^{\lambda_2} S_\lambda^{\uparrow} \, d\lambda}{\int_{\lambda_1}^{\lambda_2} S_\lambda^{\downarrow} \, d\lambda} \tag{1}$$

where $S_\lambda^{\downarrow}$ is the incident radiation at wavelength λ, $S_\lambda^{\uparrow}$ is the reflected radiation at wavelength λ, and λ_1 & λ_2 are the lower and upper wavelength limits. Albedo can thus be defined for specific *spectral* values, or as a total, *broadband value*. In the literature, the term albedo often refers to shortwave radiation (0.3 – 2.8μm), encompassing the near ultra-violet (NUV), visible, and near infra-red (NIR) regions of the electromagnetic

spectrum. Because of its importance for melting snow (Paterson, 2000), the shortwave albedo is the sole focus of this thesis and all further uses of the term albedo refer to shortwave, blue-sky albedo, unless explicitly stated otherwise.

2.1.2 Importance in the Arctic

The near-ubiquity of snow and ice is a defining characteristic of the Arctic because they are much more reflective than most natural surfaces (Figure 2). The albedo therefore determines how much radiation is absorbed by the surface: the most extreme comparison is between fresh snow and open water, with <10% of the incoming shortwave radiation being absorbed within fresh snow, whereas 90% of the radiation is absorbed by open water.

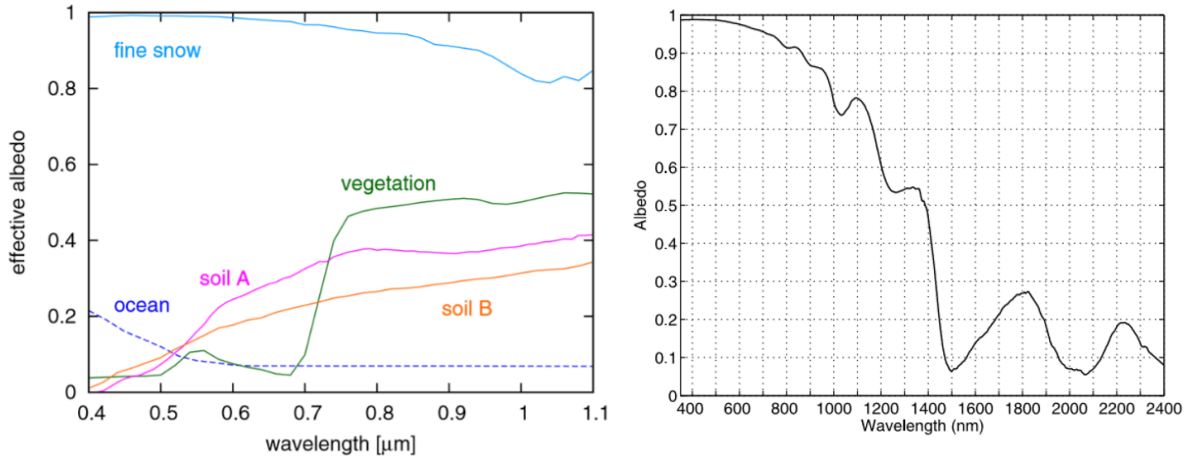

Figure 2: Comparing the spectral albedo for fine-grained snow with other common surfaces
Note that the spectral range displayed in the left-hand plot (Fuji et al., 2011) is only the lower end of the shortwave region; the full shortwave spectrum for snow is shown to the right (Hudson et al., 2006)

Albedo is particularly important for the GrIS because of the surface-albedo feedback (Sellers, 1969; Hall, 2004). In this loop, rising surface air temperatures transform the snow and lower the surface albedo (see section 2.2.4.2). This results in additional radiation being absorbed by the surface, thus perpetuating the loop. The onset of this feedback mechanism in an unusually early spring melt was a primary cause for the strong loss of ice across Greenland in 2010 (Tedesco et al., 2011), and is one of the main reasons why the Arctic is more sensitive to changes in surface air temperatures than other parts of the globe (Manabe & Stouffer, 1980).

2.2 Controls on Snow Albedo

2.2.1 Overview

A surface's albedo is determined by its physical properties, the atmospheric conditions, and the Solar Zenith Angle (SZA). To understand how each of these factors change the albedo, it is easiest to view the albedo as the net result of refraction and reflection within the snow (Warren, 1982; Jensen et al., 2001). Each of the factors described here can change the frequency and outcomes of these events, thus dictating how much of the radiation escapes the snowpack (increasing albedo), and how much is absorbed (decreasing albedo).

It should be noted that whilst this thesis is concerned with the albedo across the full shortwave spectrum, Figure 2 shows that the spectral albedos within this range vary dramatically. In general, it can be said that the spectral albedo is much higher for the shorter wavelengths.

2.2.2 Solar Zenith Angle

The SZA is the angle between the normal and the sun in the sky. A larger SZA (i.e. a lower sun) will produce a larger albedo. This can be understood because the SZA dictates the depth of a photon's first scattering event (Warren, 1982): at higher SZAs, when the photons are arriving at near grazing angles, this is much shallower, and the possibility of the photon scattering upwards and away from the snowpack is therefore greater (Figure 3). This effect is exaggerated because scattering is much more likely to happen within a few degrees of the incoming photon's direction (Aoki et al., 2000; Li & Zhou, 2004).

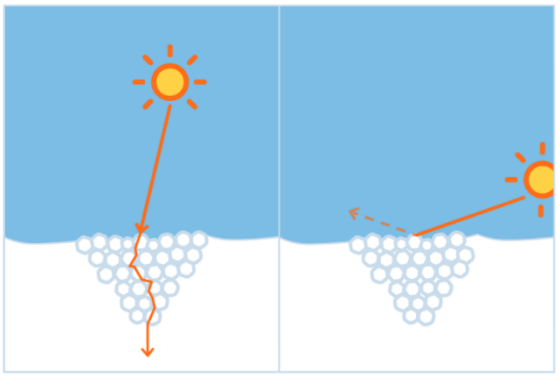

Figure 3: Schematic showing the impact of SZA on albedo

Under clear skies and with no other changes to the snow or surrounding conditions during the day, it is therefore expected that the diurnal albedo pattern is symmetrical about a noon minimum (Figure 4a), and is sometimes described in the literature as being a 'smile' (e.g. Wang et al., 2016).

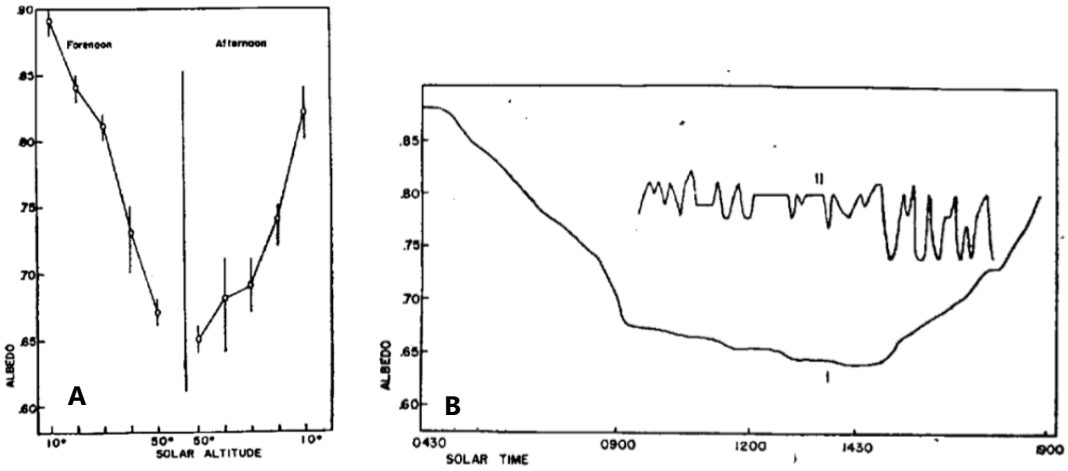

Figure 4: Diurnal albedo measurements at Lemon Creek Glacier, Alaska
(a) Average albedo against solar altitude (90°-SZA) under clear skies;
(b) Albedo for a clear (line I) and cloudy (line II) day. Source: Hubley (1955)

2.2.3 Cloud Cover

The diurnal patterns in Figure 4b illustrate the effects of cloud cover on albedo. When clouds are present (line II), the smiling pattern is lost. This is because the clouds scatter the incoming radiation, and increase the ratio of diffuse-to-direct radiation at the surface. The effect of this is equivalent to having a constant SZA of ~50° throughout the day (Warren, 1982), explaining why the smiling pattern is lost.

Cloud cover also increases the albedo. This is because the optical properties of clouds are very similar to snow, and will allow the visible wavelengths to pass through them but not the NIR wavelengths (Figure 5). The radiation that reaches the surface is therefore richer in the visible wavelengths (Grenfell & Maykut, 1977; Petzold, 1977), which have considerably higher spectral albedos (Figure 2).

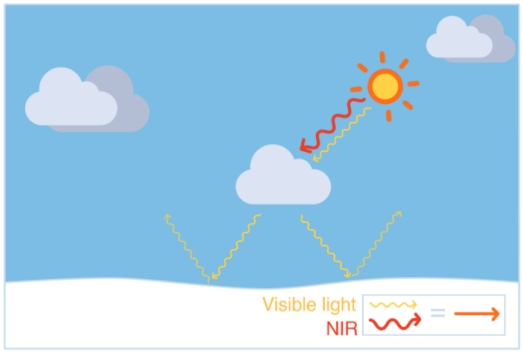

Figure 5: Schematic showing the impact of cloud cover on albedo

2.2.4 Physical Properties of the Snowpack

The exact definition of a snow grain is somewhat unclear because it is impossible to unambiguously determine where one snow grain ends and the next begins (Figure 7a). However, it is possible to measure both the volume and surface area of the entire snowpack (e.g. Shi et al., 1993) and use theoretical snow grains with an equivalent volume/surface area (V/A) ratio to optically represent the grains (Grenfell and Warren, 1999). In this way, it is possible to discuss how changes in the snow grain size affect albedo without an exact definition of what an individual snow grain is.

2.2.4.1 Snow Grain Size

Larger snow grains reduce the albedo (Painter & Dozier, 2004; Warren & Wiscombe, 1980; Figure 6). This is because photons can only be absorbed within the ice (as opposed to the air pockets), and thus larger grains increase the chance of photon absorption. Larger grains will also decrease the number of air-ice interfaces where refraction occurs and therefore decrease the chance of photons re-emerging from the snowpack (Warren, 1982). This relationship has previously been found to be proportional to the square-root of the grain size (Bohren & Barkstrom, 1974).

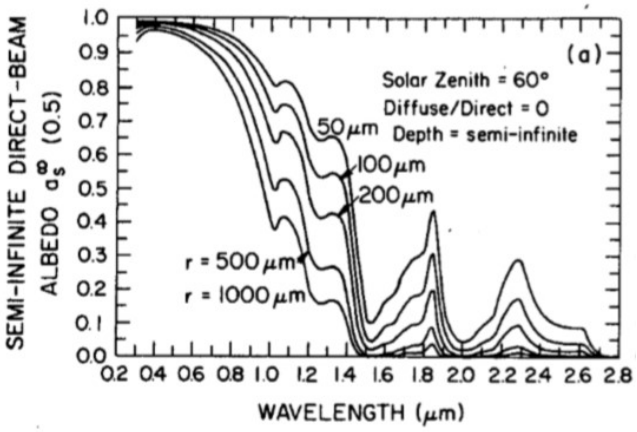

Figure 6: The impact of grain size on albedo
Source: Warren & Wiscombe (1980)

2.2.4.2 Snow Metamorphism & Grain Shape

Once snow accumulates at a surface, it will begin to metamorphose, changing both the grain size and shape. The initial metamorphism, known as *Isothermal Metamorphism*, begins immediately in fresh snow after any mechanical deformation (i.e. gravitational settling; Jordan, 1991). Differences in the vapour pressure across the grain cause sublimation at the high-pressure, convex branches, and deposition in the low-pressure concave hollows, thus rounding out the grains (Arons & Colbeck, 1995; Figure 7b). Rounder grains have a greater V/A ratio, reducing the amount of opportunities for the light to refract, and increasing the photons' probability of being absorbed. This effect rapidly decreases the albedo of fresh snow during the first day (Flanner & Zender, 2006), and will continue to occur in any isothermal snowpack (Colbeck, 1980).

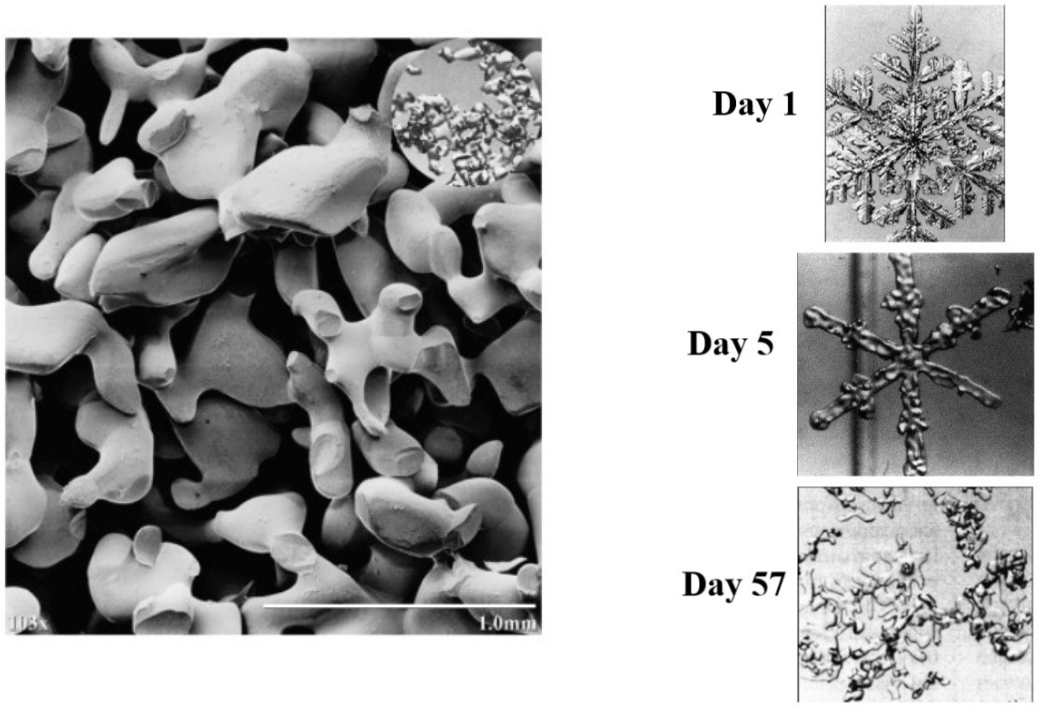

Figure 7: Snow metamorphism
(Left) Scanning Electron Microscope image of pure snow, showing the rounding of bonded grains (Dozier et al., 2009); (Right) Observations of isothermal metamorphism in the lab (Bader, 1939)

Temperature-Gradient Metamorphism occurs when water vapour transfers from a warmer layer in the snow to a colder layer (Colbeck, 1983). This produces grain shapes very different to those found otherwise, and can occur rapidly, potentially transforming up to 60% of the snow mass within 12 hours (WSL, 2018). A third type of metamorphism is also possible, called *Melt Metamorphism,* which occurs when the snowpack is at 0°C and liquid water is distributed between the grains, causing rapid growth (Brun, 1989; see section 2.2.4.3).

Both models and fieldwork experiments have confirmed that the grain shape can change albedo. For example, Leroux et al. (1998) had to replace the spherical grains assumed under the V/A approach with different shapes to reconcile their radiative transfer models with field observations. This is because the V/A ratio ignores the asymmetry of different shapes, which can determine the photons' direction within the snow (Neshyba et al., 2003; Grenfell et al., 2005). Similarly, laboratory experiments by Stanton et al. (2016) show that the near-Lambertian (i.e. perfectly diffuse) reflection of spherical grains is lost when looking at the more asymmetrical shapes of surface hoar.

In the present thesis, the firn model does not provide information on the grain shape, and thus this section is provided to highlight a potential shortcoming of the approach taken here.

2.2.4.3 Liquid Water Content & Meltwater

In snow, capillary pressure holds liquid water between the grains. This effectively increases the grain size because there is very little difference in the optical properties of ice and water in the shortwave region of the electromagnetic spectrum (Dozier, 1989). Grain clusters will also form (Colbeck, 1979), which are thought to refreeze as single, larger grains (O'Brien & Munis, 1975). Painter & Dozier (2004) report that such refrozen grains lose any preferential scattering direction, indicating that they have become more uniform and rounded: as outlined above, larger grains and greater V/A ratios decrease albedo. Brun (1989) describes the rate of grain growth in wet snow as a cubic function of LWC.

Liquid water is particularly important because it plays a significant role in the surface-albedo feedback. Box et al. (2012) suggest that this feedback can persist over multiple years if the enhanced grain growth associated with melt metamorphism corresponds with a lack of fresh snowfall, because the darkened surface effectively preconditions the ice sheet for enhanced melting in the following year.

In addition to melt metamorphism, large meltwater events will drastically reduce the surface albedo if water is trapped above impermeable layers (Dozier et al., 1981). Numerous examples of such meltwater ponds populate the literature, and the accumulation of meltwater held just beneath the surface has been used to explain the low albedo 'dark-zone' in western Greenland (Greuell, 2002).

2.2.4.4 Impurities

Impurities are parts of the snowpack that are neither ice nor air, such as black carbon, dust, volcanic ash, and algae. These reduce the albedo because they are much more absorptive than snow grains for the shorter wavelengths, and can therefore enhance grain growth and trigger earlier spring melt (Bond et al., 2013; Hansen & Nazarenko, 2004; Flanner et al., 2007). At the longer wavelengths (>~900nm), impurities cause only negligible effects because these wavelengths have often already been absorbed by the snow before they have chance to encounter the impurity (Warren & Wiscombe, 1980; Gardner & Sharp, 2010).

In addition to the size and concentration of impurities (Cook et al., 2017; Figure 8), the location of the impurity in the snow determines how much it reduces the albedo: for example, those sat within the snow grain can reduce the albedo 1.4 times further than those located in the air pockets between grains (Chylek et al., 1983).

In this thesis, impurities are not considered as they are not included in the PROMICE dataset.

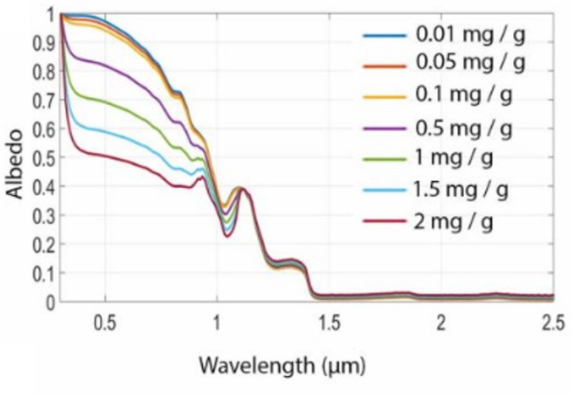

Figure 8: Modelled impact of algae concentrations on albedo
Source: Cook et al. (2017)

2.2.4.5 Other Factors – Density, Snow Depth & Roughness

Bohren & Beschta (1979) found that albedo is not dependent on snow density after they artificially compressed snow with a snowmobile, thus retaining the original grain size whilst changing its density. However, the surface roughness can be important as it may change the angle of incidence or trap radiation, particularly at high SZAs (Zhuravleva & Kokhanovsky, 2011). In this thesis, no data regarding the surface roughness is available.

Finally, the snow depth is important because it dictates whether the albedo is determined only by the snowpack, or also by an underlying surface (Warren & Wiscombe, 1980). As any underlying surface almost certainly has a lower albedo than snow, thinner snowpacks will have lower albedos: the depth at which snow is considered optically thick enough for the underlying surface to become irrelevant is discussed in terms of liquid water equivalent, with values reported to be on the order of 2 – 20 cm w.e. (Warren & Wiscombe, 1980). In this thesis, the snow depth is considered to be irrelevant because the study site is located in the accumulation zone of the GrIS, where bare ice is not revealed (section 3.1.2).

2.3 Previous Albedo Parameterisations

Whilst accurate models of snow albedo exist at the individual grain scale (e.g. SNICAR, Flanner & Zender, 2006; Warren & Wiscombe, 1980; Kokhanovsky & Zege, 2004), their complexity means that they are unable to be replicated across an ice sheet or included in regional climate models. Subsequently, numerous simplified parameterisations of snow albedo have been created, which aim to approximate snow albedo based on simpler rules from easy-to-gather parameters that can be more feasibly scaled.

There are four broad approaches to parameterising snow albedo, which can be approximately categorised as: *Fixed Value; Temperature-Dependent; Time-Dependent;* and *Coupled*. Fixed value models will not be discussed any further because they assign a set albedo value when snow is present, possibly dependent on latitude, and are therefore not a suitable approach for this thesis.

The intention of this section is not to critically analyse each of these approaches, but rather to provide a broad overview of previous parameterisations, and to act as context and inspiration for the present thesis. More detailed reviews and comparisons of snow albedo parameterisations can be found, for example, in the works of Henderson-Sellers & Wilson (1983), Barry (1996), Pirazzini (2009), Gardner & Sharp (2010), and Essery et al. (2012).

2.3.1 Temperature-Dependent

These schemes use the snow temperature (T_s) to estimate albedo. This is based on the assumption that the temperature of the snowpack drives grain evolution, because warmer temperatures can hold more water vapour and therefore increase the rate of grain growth (as outlined in section 2.2.4.1). The correlation between snow temperature and albedo allows for straightforward parameterisations, which take the form of a ramp between a minimum albedo (α_{min}) at the melting point (T_{Melt}) and a maximum albedo (α_{max}) at a defined cold temperature (T_{min}). This cold temperature has previously been defined as anywhere between -1°C (CAM2; Collins et al., 2002) and -10°C (ECHAM4; Roeckner et al., 1996).

Using the parameterisation of Roeckner et al. (2003) as an example, the albedo in such schemes can be expressed as:

$$\alpha = \alpha_{min} + (\alpha_{max} - \alpha_{\min}) * f(T_s) \quad (2)$$

where

$$f(T_s) = min\left\{max\left[\left(\frac{T_{Melt}-T_s}{T_{Melt}-T_{min}}\right), 0\right], 1\right\} \quad (3)$$

The values for α_{max} and α_{min} are determined empirically from observational studies or following the best practices of existing models. For example, the temperature-driven albedo scheme in the HIRHAM5 surface scheme model presented by Langen et al. (2015) uses α_{max} = 0.85 for fresh snow ≤-5°C and α_{min} = 0.65 for snow at T_{Melt} following van de Wal & Oerlemans (1994) and Cuffey & Paterson (2010).

In other schemes, the visible and NIR wavelengths are handled separately, with different values for α_{max} and $\alpha_{min,}$ and therefore different rates of change (e.g. Kiehl et al., 1987).

In general, temperature-dependent schemes are overly-simplistic as they lack the capability to replicate certain processes in the snow: for example, none of the schemes shown here can handle the fact that whilst temperatures can both increase and decrease, the associated grain growth is irreversible. However, because the temperature is already an output of the models that these schemes are being implemented in, such an approach provides an easy method to improve upon using a fixed value.

2.3.2 Time-Dependent

Time-dependent schemes aim to mimic the decrease in albedo seen as snow ages. Previous schemes have parameterised snow albedo as linear (Winther, 1993), exponential (Essery et al., 2012) or log (Brock et al., 2000) functions of time, based either on the number of days (Oerlemans & Knap, 1998) or cumulative surface temperatures (Klok & Oerlemans, 2004) since a snowfall. Some authors have used separate rates for wet and dry snow (Bougamont et al., 2005; Essery et al., 2012), whilst others have produced functions whose rate of change is based on the snow temperature (Reijmer et al., 2005; Figure 9).

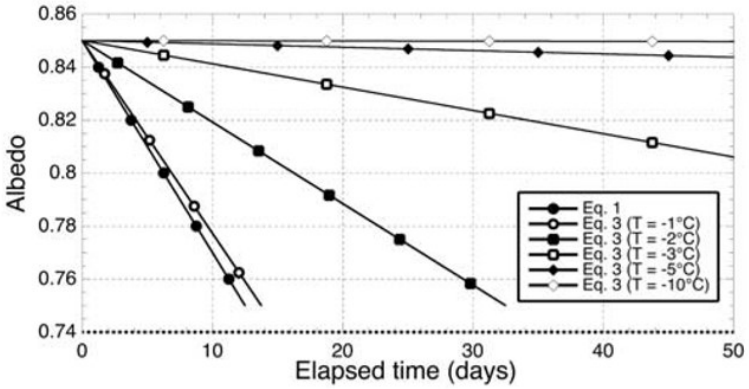

Figure 9: Temperature-dependent albedo decrease rates following a snowfall event
Source: Reijmer et al. (2005)

The complexity of time-dependent parameterisations and how they formulate the changing albedo can vary significantly between schemes. For example, the scheme of Winther (1993) uses a simple linear equation that relies on the accumulated daily maximum temperature and the incoming shortwave radiation. This scheme fits the data it was created for very well (R = 0.94; RMSE = 0.02), but it was based only on two weeks of observations.

Fitting the curves to short timescales such as this can limit the capability of time-dependent schemes being extrapolated over longer periods or applied to different locations.

Some more complex approaches try to allow for such variation. For example, the approach of Bougamont et al. (2005) expresses the rate of albedo decrease as a differential equation:

$$\frac{d\alpha}{dt} = \frac{\alpha - \alpha_{old}}{t^*} \quad (4)$$

where α_{old} is the albedo for old snow and t^* is the timescale for albedo decay in days. t^* is defined depending on the temperature and whether the snow is wet or dry. However, the exact coefficients for these still need to be determined from previous studies in the region.

2.3.3 Snow Model-Coupled Schemes

Coupled schemes incorporate the metamorphism within a snowpack directly by including the grain size, rather than using time or temperature surrogates. This means that they require output from a snow grain model, and there can be much variability in terms of their complexity and computational requirements. This subsection briefly outlines the coupled schemes from Brun et al. (1992) and Kuipers Munneke et al. (2011) as examples.

2.3.3.1 CROCUS (Brun et al., 1992)

CROCUS is dependent on the optical grain size (d). This is defined as the size of a theoretical, spherical grain with the same albedo as the real snow, and is calculated as a function of temperature, density and liquid water. CROCUS calculates the albedo for three spectral bands separately, each as a different function of $\sqrt{d}$, and then combines the three values to produce an albedo for the full shortwave spectrum.

Lefebre et al. (2003) integrate the CROCUS albedo with additional terms for snow depth, ice and meltwater in their own model, and use a cosine function to account for the SZA after Segal et al. (1991); their model does not account for the effects of changing cloud cover or impurities in the snow. Their model was compared with 2 years of field results from Greenland, and is found to replicate the albedo well even though the snow conditions were very different for each year (Figure 10 shows 1991).

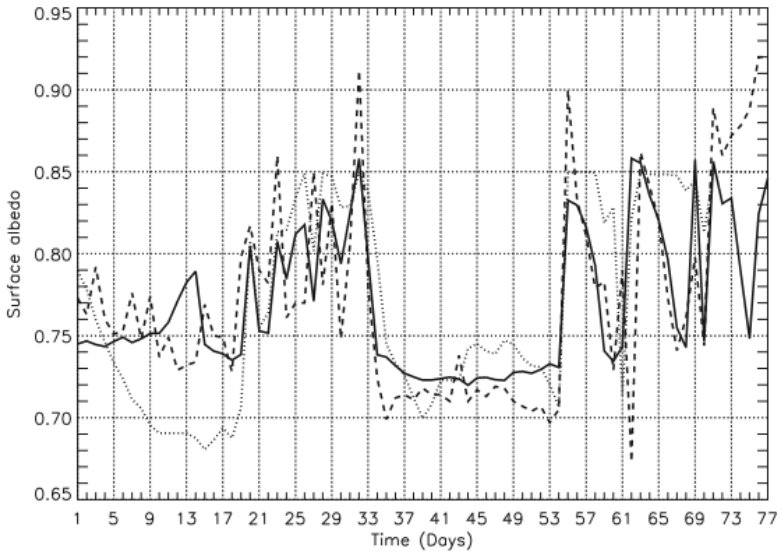

Figure 10: CROCUS-simulated (solid line) and observed (dashed line) albedo
The dotted line shows an alternative albedo model as reference. Source: Lefebre et al. (2003)

2.3.3.2 Kuipers Munneke et al. (2011)

The parameterisation of Kuipers Munneke et al. (2011) is based on that of Gardner & Sharp (2010) but uses a grain size calculated by the SNICAR radiative transfer model (Flanner & Zender, 2006). This is incorporated by fitting a parametric curve to the SNICAR output as it is too computationally-expensive to calculate this within the scheme.

The SNICAR grain size is used to determine a 'base' albedo, which is then modified by adding individual terms to explain the effects of impurities, the SZA and cloud cover on the albedo, as:

$$\alpha = \alpha_{SNICAR} + \alpha_{SZA} + \alpha_{IMPURITIES} + \alpha_{CLOUDS} \quad (5)$$

Kuipers Munneke et al. (2011) incorporated this parameterisation into a regional climate model over Antarctica, and report that it captured the subtle variability of in-situ albedo observations well, but note that an adjustment needs to be made to account for the optical thickness of the atmosphere.

It is the intention of this thesis to create a snow model-coupled scheme, using the grain size calculated by the firn model.

3 Datasets

3.1 PROMICE

The Programme for Monitoring the Greenland Ice Sheet (PROMICE) maintains a network of ~22 automatic weather stations across the GrIS (Ahlstrøm et al., 2008). Each station consists of a barometer, thermometer, anemometer, radiometer, sonic ranger, pressure transducer, thermistor string, inclinometer, and GPS antenna. Measurements are made every 10 minutes, with averages transmitted hourly during the summer (days 100-300) and daily in winter.

For this thesis, the key variables measured by the station are the incoming and outgoing shortwave radiation because these variables define the surface albedo. This provides an observational dataset that is compared with the output from the firn model. Additionally, longwave radiation measurements are used to determine the cloudiness (section 4.2.2), whilst the temperature, precipitation, relative humidity, air pressure, and wind speed were used as input for the firn evolution model.

3.1.1 Radiometers

Incoming and outgoing shortwave and longwave radiation are measured with a Kipp & Zonen CNR4 net radiometer (Kipp & Zonen, 2018). This consists of an upward- and downward-facing pair of pyranometers to record shortwave radiation, and an upward- and downward-facing pair of pyrgeometers to record longwave radiation.

The pyranometers operate at 300-2800nm, with a nearly-uniform sensitivity over this spectral range (Figure 11). The overall uncertainty in the daily total is <5%. The upward-facing pyranometer has a 180º field of view, whereas the downward-facing pyranometer is restricted to 150º to prevent direct illumination at low SZAs. It is explicitly stated in the manual that that these sensors are not suitable for calculating albedo at SZA>80º because deviations in the directional response of the instrument make the results unreliable. The implications of this for the dataset are explained below (Section 3.4).

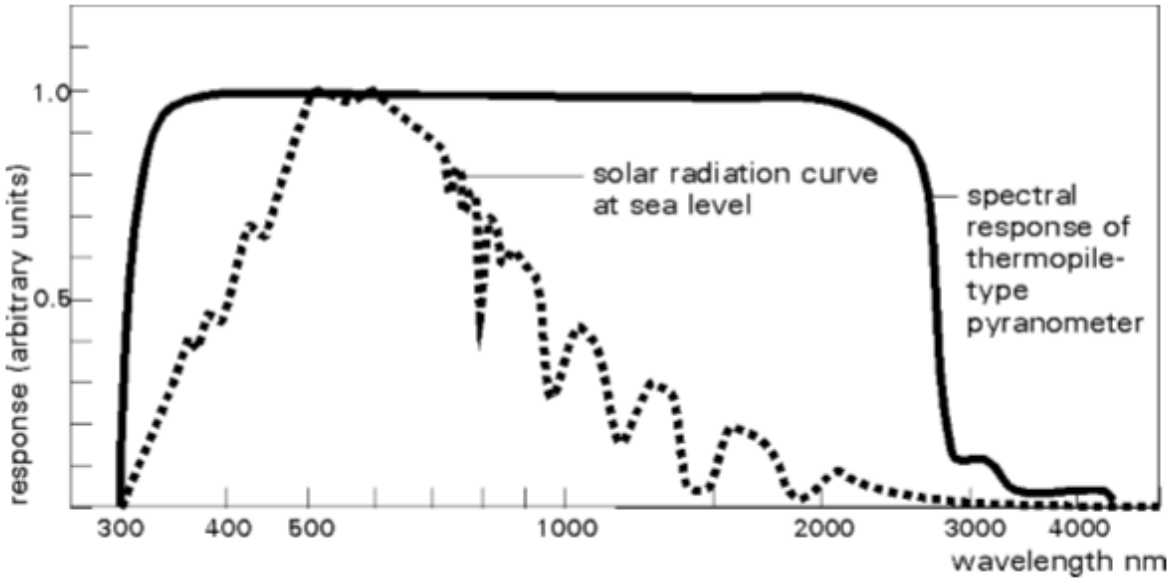

Figure 11: Pyranometer spectral sensitivity under a clear sky
Source: Kipp & Zonen (2018)

The pyrgeometers record longwave radiation from 4.5-42μm, with an overall uncertainty in their daily totals of <10%. They are constructed to account for errors that would arise from their own temperature. Further details on the radiometers can be found in the CNR4 manual, accessible via the Kipp & Zonen webpage listed in the references. All weather station data was processed by Charalampidis et al. (2015), including tilt corrections for radiation measurements as in Van As (2011).

3.1.2 Kangerlussuaq Upper Station

Kangerlussuaq Upper (hereafter KAN_U) is a PROMICE weather station located in the lower accumulation zone of the Kangerlussuaq region of western Greenland (67.0003°N, 47.0253°W; Figure 12a). It sits approximately 140km inland of the ice margin, at an elevation of 1840m.a.s.l. The equilibrium line altitude for the Kangerlussuaq region, where annual accumulation and ablation are equal, is ~1550m.a.s.l (van de Wal et al., 2012), and superimposed ice reaches no higher than ~1750m.a.s.l. (van den Broeke et al., 2008). This means that any melt at KAN_U will not reveal bare ice.

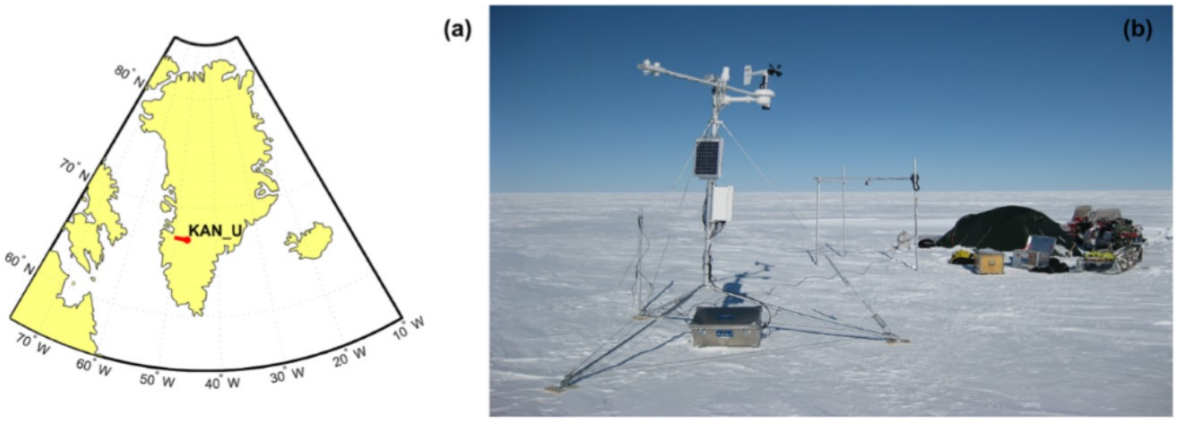

Figure 12: KAN_U Weather Station
(a) Location within Greenland (b) Immediately after installation in April 2009
Source: Charalampidis et al. (2015)

In addition to its relatively long dataset (April 2009 onwards), KAN_U was selected as the focus of this parameterisation because scientific interest in the high-altitude regions of the GrIS has increased since 2012, when large surface meltwater fluxes from the accumulation zone were reported (Charalampidis et al., 2015). It is normally expected that any meltwater at such elevations will refreeze, restricting any contributions to sea level rise. However, in 2012, the unusually high temperatures and limited precipitation resulted in layers of refrozen firn that subsequently trapped meltwater at the surface, significantly reducing the albedo and leading to further melt (Charalampidis et al., 2015) and increased runoff.

3.2 Firn Evolution Model

The firn evolution model (Vandecrux et al., in review) was used to provide the grain size, density, and liquid water content (LWC) of the snow. This thesis is only concerned with data from the surface layer of the model (<10cm w.e.).

3.2.1 Grain Size, Density & LWC

The model prescribes fresh snow with an initial grain diameter of 0.1mm, as in Katsushima et al. (2009). For low LWC (<~6%), the grain's subsequent growth rate is calculated as function of the LWC and current grain

size, using the work of Brun (1989). Above this LWC threshold, the growth rate no longer relies on the LWC, but is purely a function of the grain's current diameter.

LWC is calculated based on the temperature of the snow, with the energy from any temperature rise that would go above 0°C being used to melt the snow. The irreducible water content of the snow, which is the water that can be held in place by capillary tension between the grains, is also accounted for, based on a relationship with porosity that was found by Coleou & Lesaffre (1998).

The density of fresh snow in the model is set at 315kg/m^3 after Fausto et al. (in review), and the rate of densification is calculated as a function of the overburden pressure and snow viscosity, following Vionnet et al. (2012).

Further details regarding the model can be found in Langen et al., (2015), Langen et al. (2017) and Vandecrux et al. (in review).

3.3 Additional Parameters

3.3.1 SZA

The SZA was calculated using a MATLAB function that required only the local time and latitude as input (Mikofski, 2013). Random tests of these values were compared against the solar calculator used by the National Oceanic and Atmospheric Administration (NOAA, 2018): values were found to be within ±0.5º in almost all cases, except for at the very highest SZA (>75º) where differences occasionally surpassed ±1º. The SZA was calculated at the midpoint of each hour (i.e. 08:30) to reflect that the PROMICE data was an hourly average. The validity of this choice is discussed in Chapter 6.

3.3.2 Snow Conditions

Each time step was categorised as one of three distinct snow conditions to facilitate understanding of the effects of meltwater and refreezing on the snow albedo.

Aged snow refers to fresh snow that ages without ever containing any LWC; *refrozen* snow is snow that has previously contained LWC but subsequently refrozen; and *wet s*now is snow that contains LWC in the current time step. The LWC values used to define this were calculated by the firn model; snowfall was defined from the PROMICE data.

3.4 Constraining the Dataset

To mitigate against the inaccuracies of the radiometers at high SZAs, a maximum SZA threshold was implemented. This restricts the applicability of the parameterisation to certain conditions. However, whilst the aim of the thesis is to parameterise snow albedo, this has the underlying motivation of improving the representation of radiative energy exchanges at the ice sheet. At the very highest SZAs, the amount of incoming shortwave radiation (SR_{IN}) is comparatively low and unlikely to cause melt or greatly enhance metamorphism in the snow. For example, approximately 26% of the total SR_{IN} during the entire 8-year dataset occurs at SZAs > 70º; this falls to 9.5% for SZAs > 80º (Figure 13).

Previous authors have used different thresholds between 65º and 80º to constrain their investigations (e.g. Pirazzini, 2004; Stroeve et al., 2006). It was decided here that using a SZA threshold of 65° or 70º would exclude a significant proportion of the data that had important implications for radiative energy exchanges, and therefore a maximum SZA threshold of 80º was used. However, this boundary was chosen with the awareness that the mean cosine error of the radiometers approximately doubles from ~2% to ~4.5% between 70º and 80º (Kipp & Zonen, 2018), and thus such data should be treat cautiously. A minimum SR_{IN} value of 50W/m^2 was also implemented to catch any low-radiation data missed by the SZA threshold.

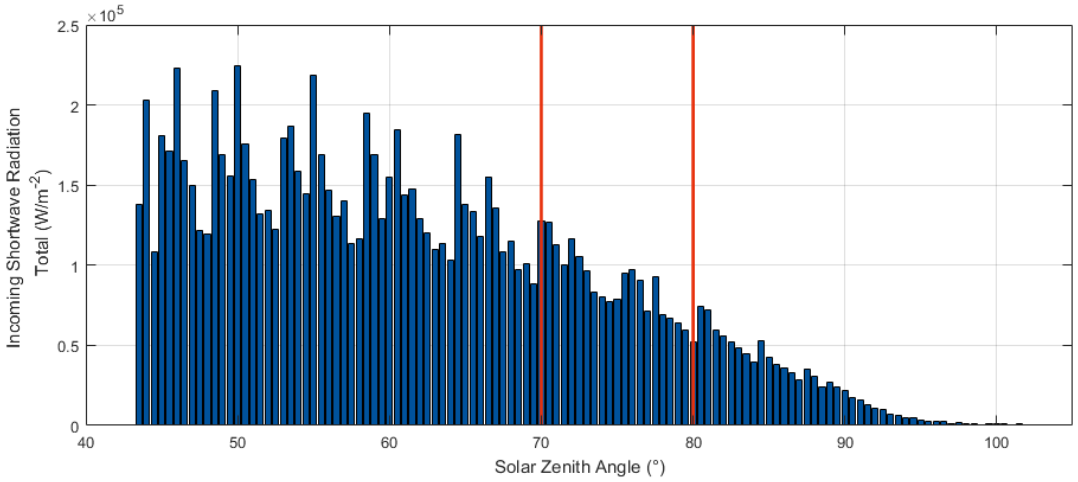

Figure 13: Sum of incoming solar radiation for different SZAs over the entire dataset

Finally, it was decided to use only data from the summer when hourly data was available (days 100-300). This condition excluded the dark polar winter, and ensured that the parameterisation was tuned to replicating the albedo when it was the most meaningful for the snow.

Table 1: Constraints applied to the data used in this thesis

Constraints
Incoming Solar Radiation > 50W/m^2
Solar Zenith Angle < 80°
Summer (Days 100 – 300)

4 Methodology

4.1 Overview

This chapter details the methodology used to uncover and quantify relationships between the observed albedo dataset and parameters from the firn model. Preliminary sensitivity analyses (not shown) revealed much inter- and intra-annual variation in correlations, and it was decided to separate the dataset into subsets with different characteristics.

An initial separation was made between clear and cloudy skies, identifying when the SZA was most important. Wet and dry snow were also handled separately, with a further distinction made in the dry snow between snow that had always been dry (*aged* snow), and snow that had previously contained liquid water but subsequently refrozen (*refrozen* snow).

Following the literature review, it was decided to restrict the analysis to explaining the albedo with the SZA, the snow grain size, the LWC, and a proxy for cloudiness (SATR). Relationships with other variables are occasionally reported here but were avoided as they were unexplainable or considered to be surrogate values that couldn't be untangled; they are included here to provide context for a discussion in Chapter 6.

4.2 Clear and Cloudy

4.2.1 Identifying Diurnal Albedo Patterns

Under clear skies, the diurnal albedo pattern is driven by the SZA. When clouds are present, this pattern is lost, and thus it should be possible to use the diurnal patterns of the observed albedo to identify clear and cloudy skies. Examining the dataset revealed three distinct patterns, here termed as 'Linear Rises', 'Squiggles' and 'Smiles' (Figure 14). Approximately half of the ~1600 days examined could be separated into one of these three categories: the remaining half had inconsistent patterns that were expected to be the result of changing cloud conditions, and were excluded from this initial analysis.

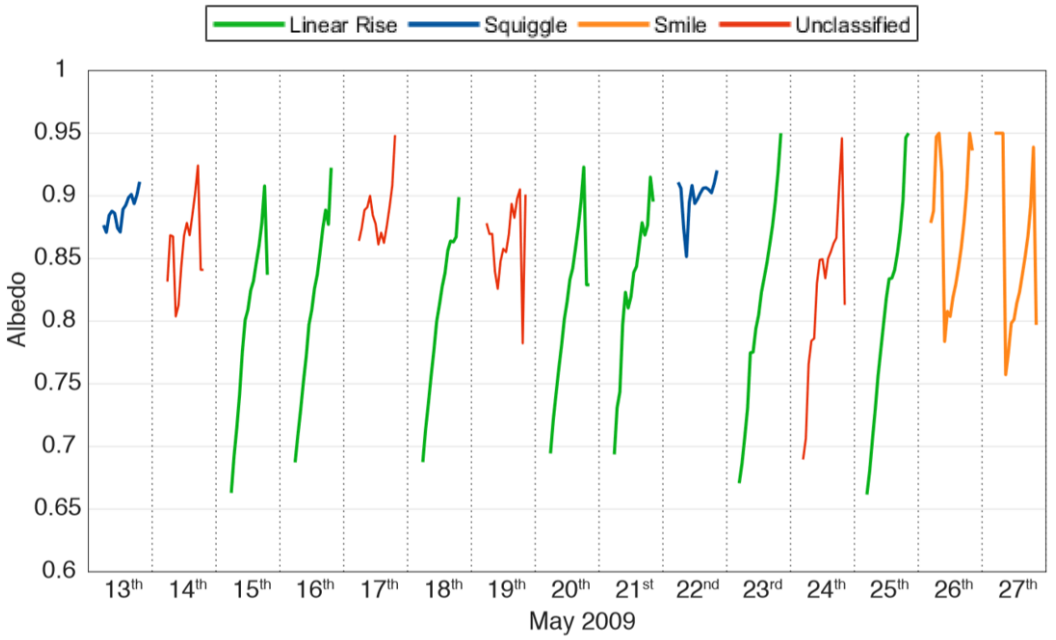

Figure 14: Identifying diurnal albedo patterns in the PROMICE observations (Example from May 2009) The albedo is plotted against the local time for each day

4.2.2 SATR: The Sky-Air Temperature Ratio

To understand how these observed patterns related to different cloud cover conditions, they were compared to the Sky–Air Temperature Ratio (SATR). This is a proxy for the cloudiness that relies on the incoming longwave radiation (LR_{IN}) measurements made at KAN_U.

Under the assumption of blackbody radiation, the temperature of an object determines the amount of radiation that it emits:

$$Emitted\ Radiation = T^4 * \sigma \tag{6}$$

where σ is the Stefan-Boltzmann constant ($5.67*10^{-8}$ W m^{-2} K^{-4}). This equation can be expressed for our purposes as:

$$LR_{IN} = T_{SKY}^4 * \sigma \tag{7}$$

where LR_{IN} is the incoming longwave radiation, and T_{SKY} is the sky temperature. This can be rearranged as:

$$T_{SKY} = \left(\frac{LR_{IN}}{\sigma}\right)^{\frac{1}{4}} \tag{8}$$

Under clear skies, T_{SKY} is much lower than the air temperature (T_{AIR}) recorded at the weather station, because the radiation emitted by the Earth is lost to space. When clouds are present, this radiation is trapped and reradiated back to the surface (i.e. LR_{IN}), making T_{SKY} higher and much closer to T_{AIR}. The ratio between T_{SKY} and T_{AIR} can therefore be used as a proxy for cloudiness:

$$SATR = \frac{T_{SKY}}{T_{AIR}} \tag{9}$$

4.2.3 SATR Boxplots

The average daily SATR value was calculated for each of the days identified as belonging to one of the three diurnal patterns. Boxplots of the SATR distribution for these patterns show that there is a clear separation between the Linear Rises and Squiggles (shown in blue in Figure 15).

It is immediately apparent that the Linear Rises have very low SATR values, indicating that they occur under very clear skies, and that the Squiggles have high SATR values, and thus represent cloudy conditions. The smiling patterns, which were expected to indicate clear skies from the literature, have a wider range of SATR values, and spread between the clear and cloudy distributions.

Boxplots of the hourly SATR values from each of the days were also plotted (shown in green in Figure 15). These understandably show a slightly larger range than the daily averages, but maintain the clear separation between the Linear Rises and Squiggles, indicating that the SATR can be used to differentiate between clear and cloudy conditions on an hourly basis.

To understand the smiling patterns, plots of the diurnal SATR and albedo were made (Figure 16). These show a definite tendency for the mornings of the smiling days to begin with cloudier skies, which then become clearer later in the day. This shows how large and immediate the impact of clouds can be on albedo.

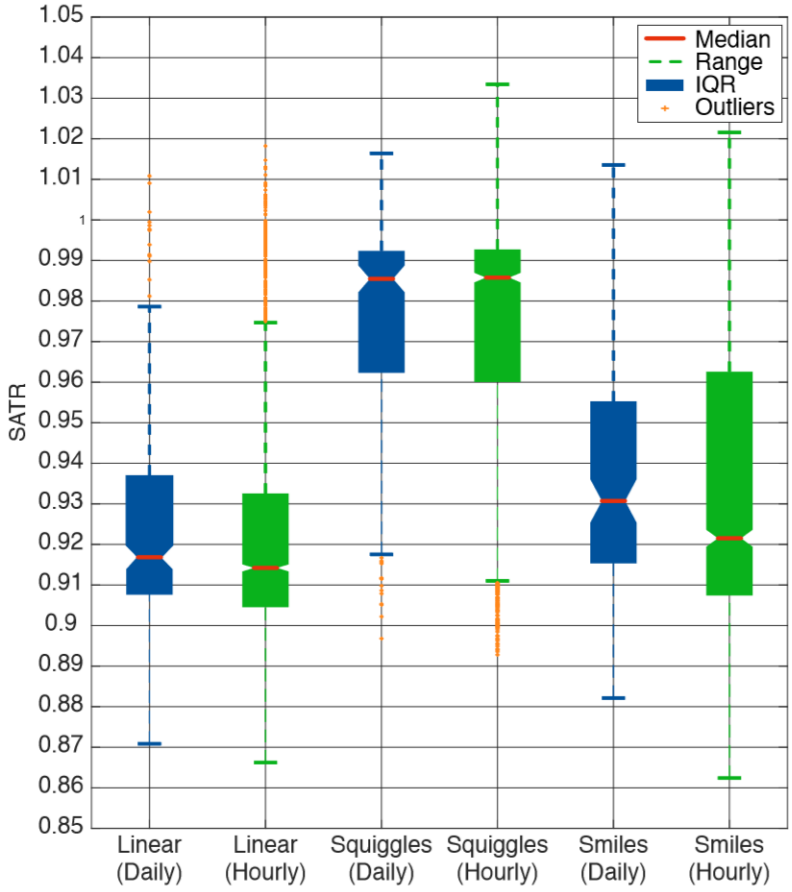

Figure 15: Boxplot of SATR values for each of the three diurnal albedo patterns
Daily averages are in blue and hourly values in green.
Outliers are values outside 3 median absolute deviations

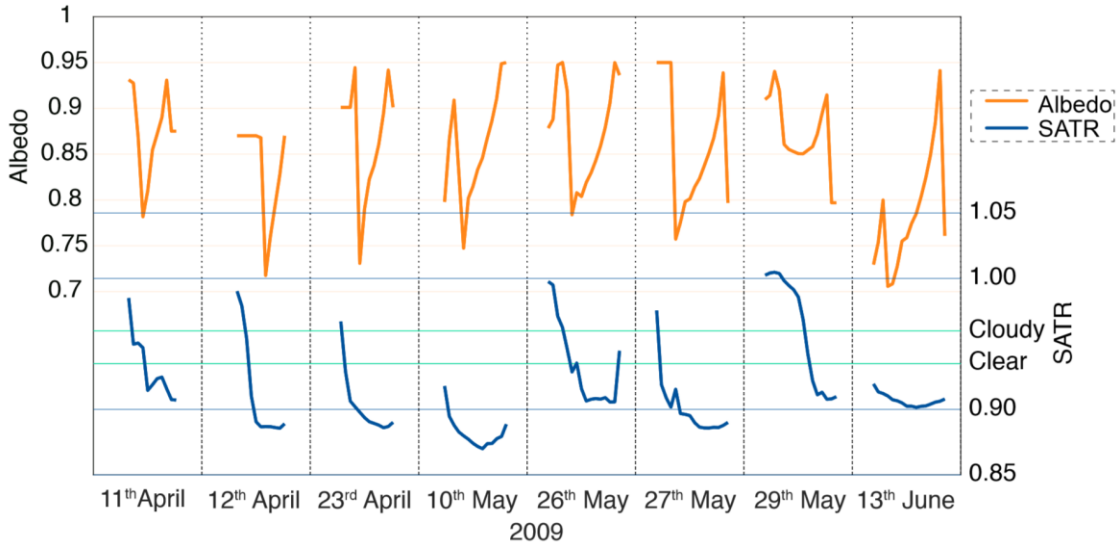

Figure 16: Examples of SATR & albedo for smiling days
Values are plotted against the local time. Clear & cloudy labels on the SATR axis represent the median value from the boxplots.

4.2.4 Defining Cloudy and Clear Thresholds

In the methodology used here, it was necessary to define a threshold at which the SATR was no longer relevant and the sky could be considered 100% cloudy. This was approached using a linear regression analysis between the observed albedo, and the SZA, SATR and grain size variables. The linear regression analysis was repeated using different minimum SATR thresholds to define 100% cloudy skies, so that only the data from hours with a SATR above the threshold were included (Figure 17). It was hoped that this would identify a point at which further increases in the SATR could be considered noise in relation to the albedo, and thus the albedo's relationship with grain size would be at a maximum, and at a minimum with the SZA.

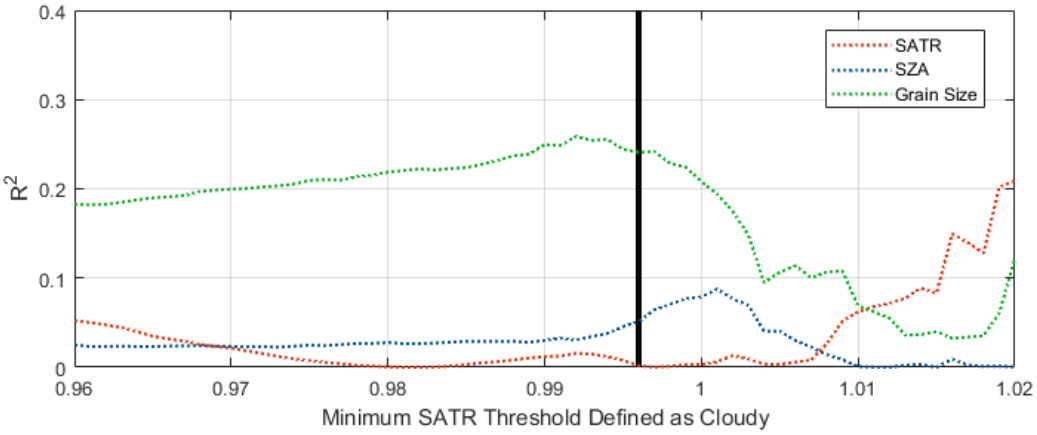

Figure 17: Determining a SATR threshold for 100% Cloudy Skies
Values on the X-axis show the minimum SATR threshold at which the sky was considered 100% Cloudy
The black line identifies the limit that was selected (SATR = 0.996)

A value of 0.996 was selected as it was judged that this could definitely be considered extremely cloudy, but would still include enough data (>1700 hours) to make any relationships statistically significant. The circular nature of this definition and its validity plus implications for the parameterisation are discussed in Chapter 6. A threshold of 0.914 was chosen in a similar way for 100% clear skies.

4.3 Albedo under 100% Cloudy Skies (SATR > 0.996)

As the definition for 100% cloudy skies is that the albedo is independent of the SZA and SATR, any variation in the observed albedo should be explainable with regressive analyses of the remaining variables. These were calculated separately for each of the three snow conditions (Table 2).

Table 2: Selection of R^2 values for listed variables and observed cloudy sky albedo

	Wet Snow Albedo	Refrozen Snow Albedo	Aged Snow Albedo
Density	0.266	0.086	0.004
Grain Size	0.256	0.153	0.005
LWC	0.216	-	-
Sublimation	0.131	0.158	0.217

All values are statistically significant at $p < 0.001$

4.3.1 Aged Snow

Table 2 shows that none of the variables can explain the albedo variation within aged snow, except for sublimation. As will be discussed in Chapter 6, it was decided that a relationship with the sublimation could not be physically justified, and therefore it was considered that the least unreliable approach for modelling the cloudy sky albedo of aged snow was to use the mean value (α=0.86).

4.3.2 Refrozen Snow

Table 2 shows that the albedo of refrozen snow has relationships with the grain size and snow thickness. Figure 18 indicates that there is a negative correlation between the grain size and the albedo, which can be partly described with a linear fit (equation 10).

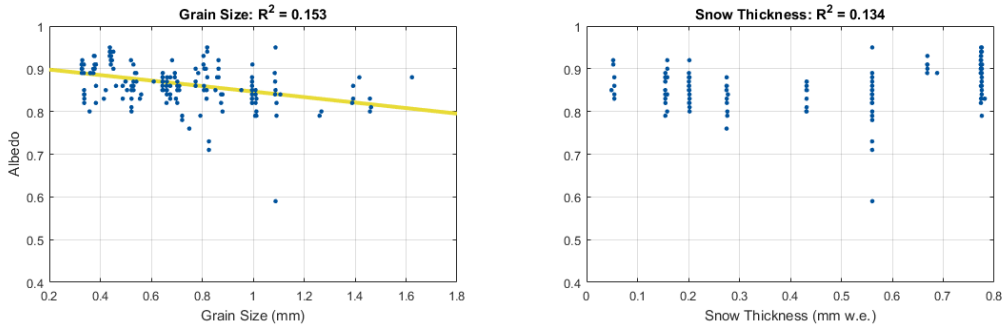

Figure 18: Scatter plots of cloudy sky albedo for refrozen snow

The yellow line in Figure 18 follows the form of:

$$\alpha = 0.911 - 0.0644d \tag{10}$$

where *d* is the grain size, in mm. This produces an RMSE value of 0.044.

The residuals between equation 10 and the observed albedo were compared against the remaining variables. Scatter plots (examples in Figure 19) showed that the distribution of the residuals was almost completely independent of all other variables (R^2 values < 0.05 and p values > 0.1). This indicates that no more of the observed albedo variation can be explained, and that equation 10 is not more suited to certain meteorological conditions than others. The cloudy sky albedo of refrozen snow is therefore expressed in this parameterisation with equation 10.

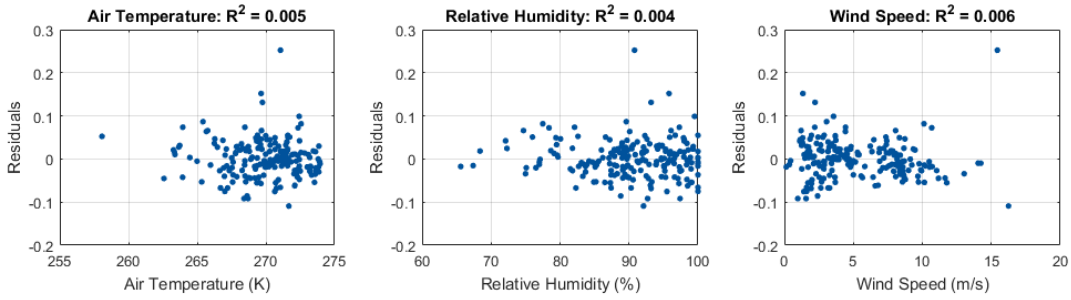

Figure 19: Example scatter plots of cloudy sky albedo residuals with Eq.10 (refrozen snow) Values on the y-axis are the difference between the observed albedo and Eq. 10

4.3.3 Wet Snow

The same approach was used for wet snow albedo. Initial relationships were identified with density, grain size and LWC (Table 2). The fits for density and grain size were almost identical to each other, and therefore it was decided to continue expressing the albedo in terms of the grain size. A clear negative correlation between grain size and the observed albedo can be seen in Figure 20. This is expected from the literature.

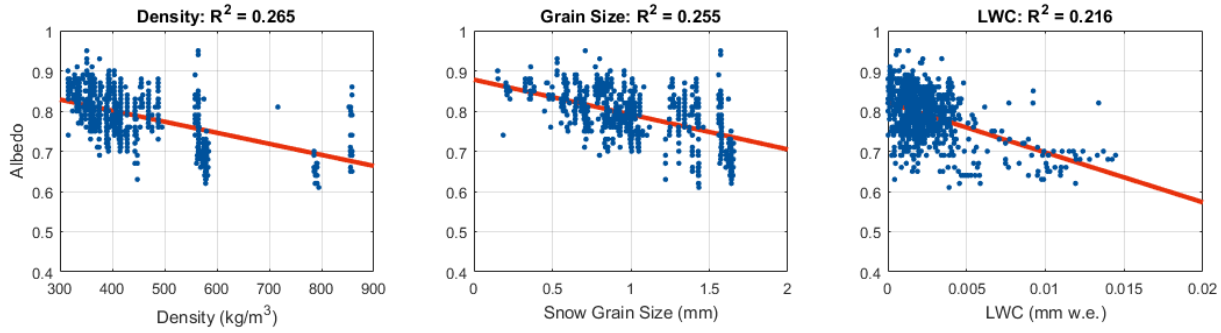

Figure 20: Scatter plots of cloudy sky albedo for wet snow
Y-axis values are the observed albedo

The red line in the middle plot of Figure 20 can be written as:

$$\alpha = 0.878 - 0.0867d \tag{11}$$

This produces a RMSE of 0.055, and $p < 0.001$. The residuals between equation 11 and the observed albedo were compared with the remaining variables. This revealed an understandable dependence on the LWC ($R^2 = 0.155$; Figure 21).

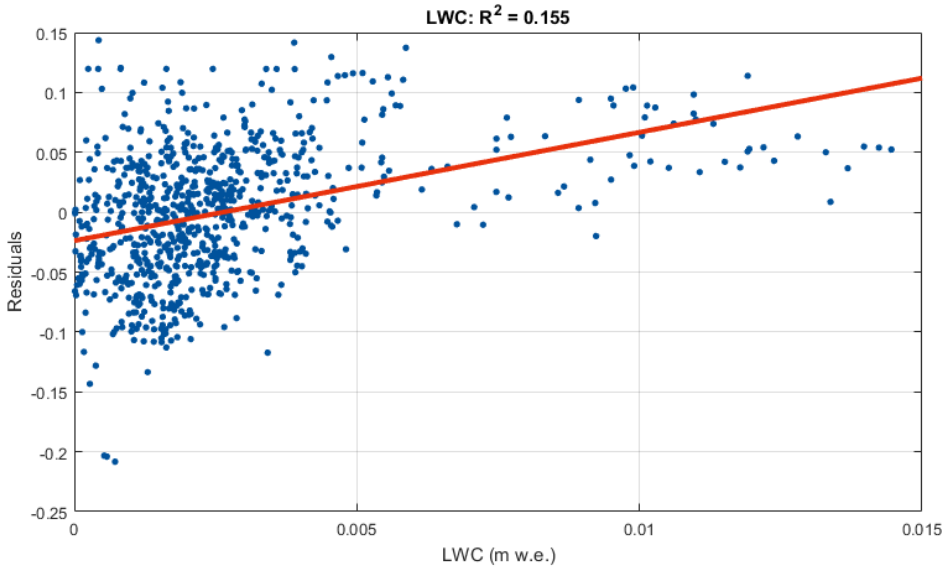

Figure 21: Scatter plot of residuals for cloudy sky albedo (wet snow)
Y-axis values are residuals between eq. 11 and the observed albedo. Positive values are model overestimates

The equation identified in Figure 21 explains the residuals as a linear function of LWC:

$$\alpha_{residuals} = -0.0236 + 9.05lwc \quad (12)$$

Equations 11 and 12 can then be combined to explain the cloudy sky albedo of wet snow as:

$$\alpha = 0.902 - 0.0867d - 9.05lwc \quad (13)$$

where lwc is the liquid water content in m w.e. The fit of this function is displayed in Figure 22 (R^2 = 0.375; RMSE = 0.05).

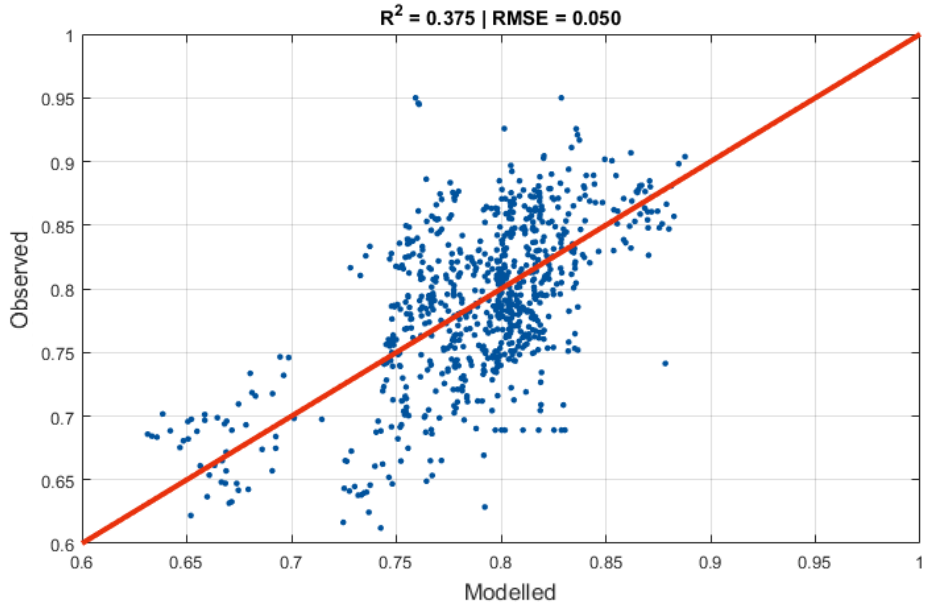

Figure 22: Modelled and observed cloudy sky albedo for wet snow

Thus far, three rules have been created to explain the cloudy sky albedo. These are used in the final parameterisation.

4.4 Albedo under 100% Clear Skies (SATR < 0.914)

As outlined in Chapter 2, it is expected that the albedo under a clear sky is driven by the SZA and will produce a smiling pattern. However, the albedo observations here revealed there was usually a linear rise for clear skies. It was therefore decided to treat the mornings and afternoons separately, but still attempt to explain the diurnal pattern as a function of the SZA. This is discussed in Chapter 6.

4.4.1 Unexpected Mornings

4.4.1.1 Aged Snow

The variation in cloudy sky albedo for aged snow could not be explained by the modelled grain size (Section 4.3.1). It was therefore assumed that the modelled grain size would not drive any change in the clear sky albedo, and that any variation would be purely described as a function of the SZA. This was verified as well

as possible by plotting the observed albedo values against the SZA for different grain sizes (Figure 23). These plots show little verifiable difference between the SZA-albedo relationship for different grain sizes.

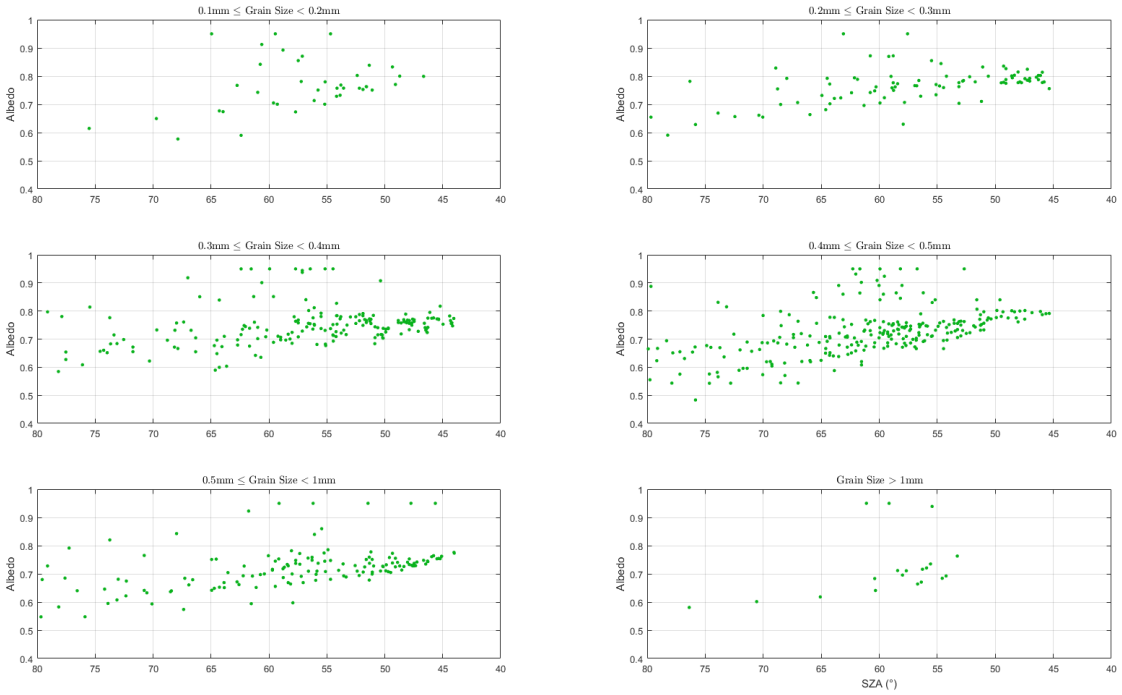

Figure 23: Hourly clear sky albedo and SZA for different grain sizes (aged snow)

It was therefore necessary to explain the observed albedo variation of aged snow only as a function of the SZA. Figure 24 is a plot of the observed albedo against the SZA, plotting only mornings in which all hours were considered to have 100% clear skies. This shows that there is a representative pattern for the clear sky albedo of aged snow, particularly if the very short days in October are ignored.

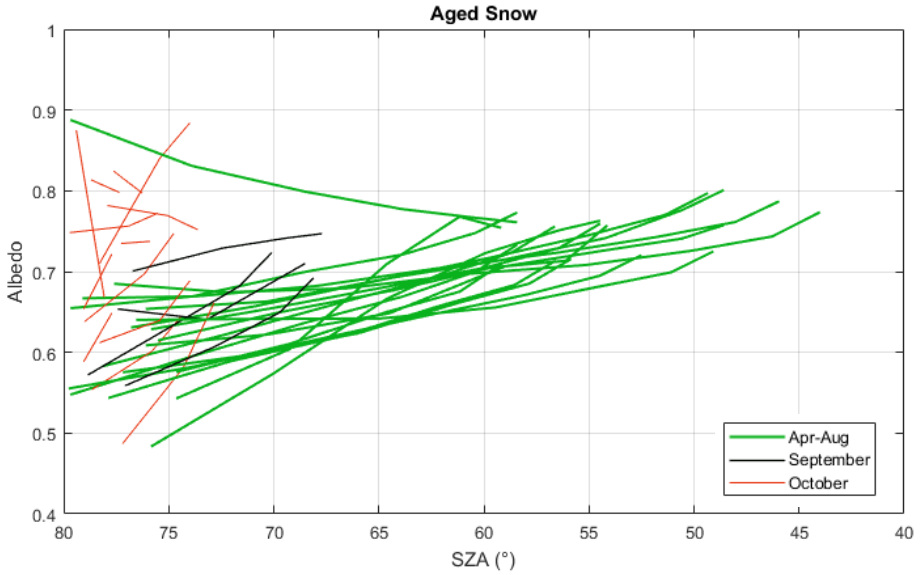

Figure 24: Clear sky albedo as a function of SZA for aged snow (mornings)
Each line depicts a separate morning in which every hour was considered a clear sky

Previous authors have used cosine fits to explain the SZA relationship with albedo (e.g. Segal et al., 1991; Gardner & Sharp, 2010), and thus a cosine fit was used here:

$$\alpha = 1.27 \ -\frac{2}{3}\cos(90° - z) \tag{14}$$

where z is the SZA in degrees.

Figure 25 compares equation 14 with all the clear hours (i.e. any hour in the mornings considered clear, irrespective of whether the rest of the morning was clear or cloudy – Figure 24 only showed the albedo when the full morning was considered clear, to identify if there was a clear diurnal pattern).

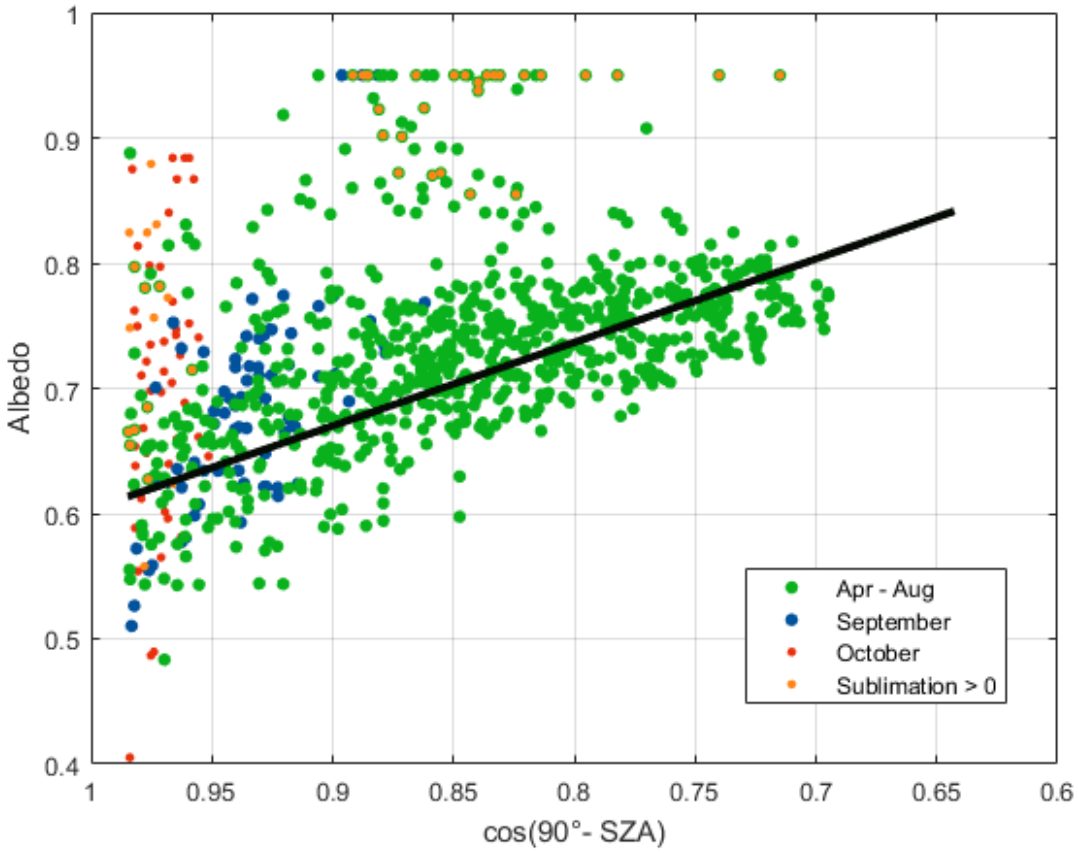

Figure 25: Hourly clear-sky albedo as a cosine function of SZA for aged snow (mornings)

Figure 25 shows that equation 14 can explain some of the clear sky albedo variation for aged snow (R^2= 0.165; RMSE = 0.075). It is noted that many of the very high albedo values seen in the figure occur when sublimation exceeded deposition (shown in orange); excluding these and the October days would improve the fit to R^2= 0.246 (RMSE = 0.062).

The residuals between equation 14 and the observed albedo were independent of any other variables, and therefore the parameterisation expresses the clear sky albedo for refrozen snow in a morning with equation 14.

4.4.1.2 *Refrozen Snow*

Figure 26 plots the observed clear sky albedo for refrozen snow. The shallower gradient and weaker fit in this plot compared to Figure 24, show that the albedo is less dependent on the SZA for refrozen snow than it is for aged snow.

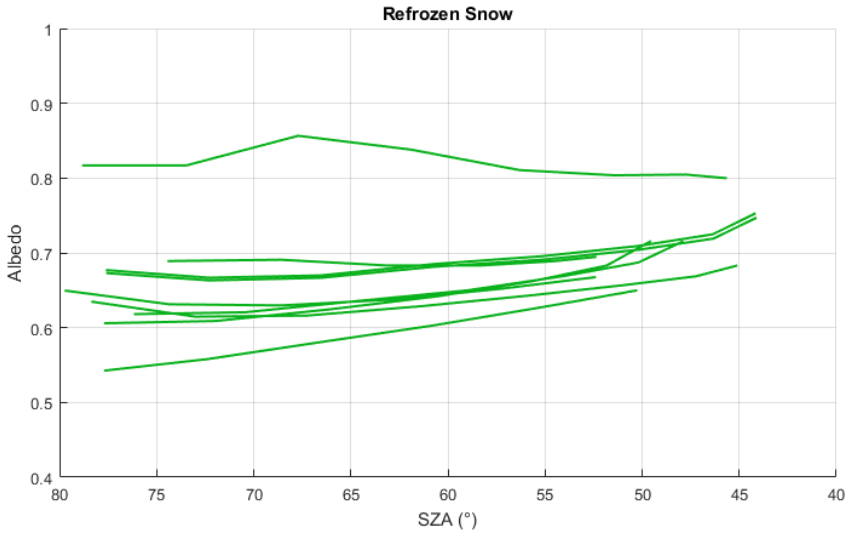

Figure 26: Clear sky albedo as a function of SZA for refrozen snow (mornings)
Each line depicts a separate morning in which every hour was considered a clear sky

The observed albedo values were compared to the cloudy sky albedo parameterisation created for refrozen snow (equation 10). A plot of the residuals from this comparison shows there is some dependence on the SZA (R^2 = 0.119; Figure 27).

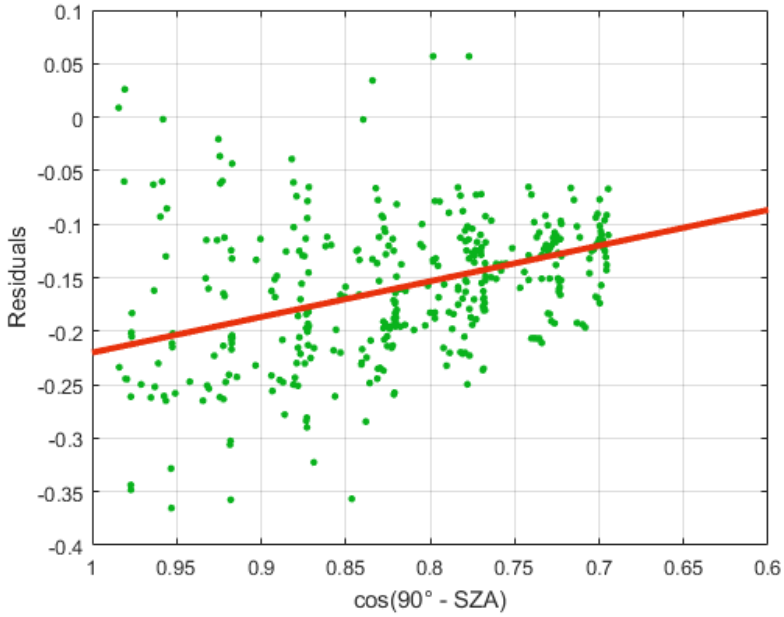

Figure 27: Residuals of clear sky albedo for refrozen snow as a cosine function of the SZA
Y-axis values show the residuals between the cloudy sky albedo parameterisation for refrozen snow, and the observed clear sky albedo for refrozen snow

It was therefore possible to modify the cloudy sky albedo parameterisation (equation 10) to incorporate the SZA dependence seen in Figure 27, and write the clear sky albedo for refrozen snow in a morning as:

$$\alpha = 0.97 \ -\frac{1}{3}\cos(90° - z) - 0.0644d \tag{15}$$

4.4.1.3 Wet Snow

There is little data available to consider clear sky albedo for wet snow in the mornings as the snow is almost always too cold for liquid water (only 90 hours over 8 years). It was therefore deemed inappropriate to base a separate parameterisation on this limited dataset and a mean value was used instead (α = 0.67).

4.4.2 Unexplained Afternoons

The plots used for the clear mornings were replicated in the afternoons. These revealed the existence of peak values in the late afternoon, after which the observed albedo rapidly dropped. This was apparent for each of the three snow conditions (shown for aged snow in Figure 28).

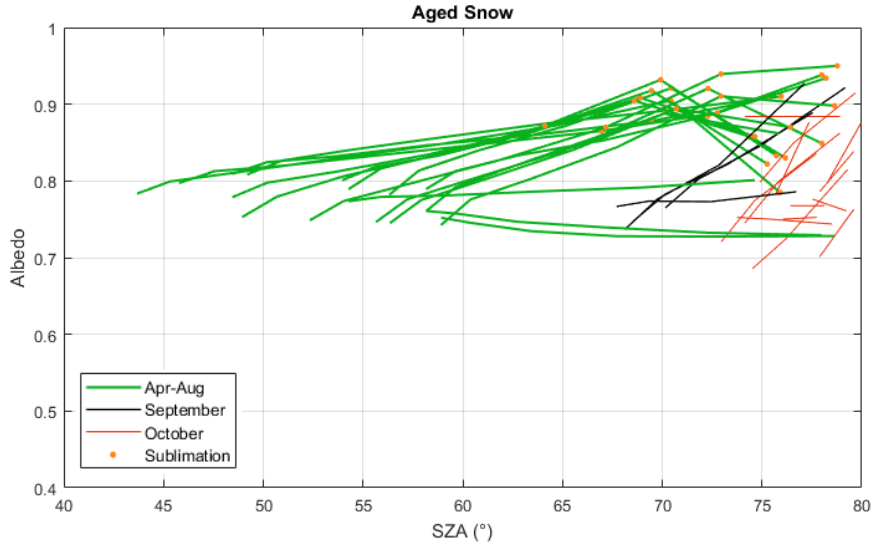

Figure 28: Clear sky albedo as a function of SZA for aged snow (afternoons)
Each line depicts a separate afternoon in which every hour was considered a clear sky

These peaks all occurred at SZAs greater than ~65°-70°, but there was otherwise no consistency between them. It was hypothesised that the peaks would align with varying weather conditions, and could, for example, be representative of shadowing effects or specific conditions in which the sensor became unreliable. However, attempts to explain the timing of the peaks with the weather station variables were unsuccessful.

Figure 29 shows an attempt to align the peaks with the hours in which sublimation exceeded deposition. Although this aligns perfectly for two of the days shown, this was not consistent across the dataset, and could not be used as a rule. Other variables were approached in the same way (not shown), such as wind speed, air temperatures, incoming/outgoing radiation thresholds, and solar azimuth ranges.

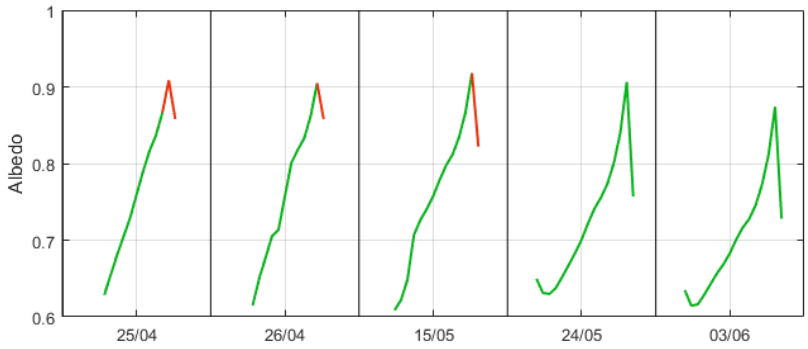

Figure 29: Afternoon peaks under clear skies
Each line depicts the Albedo for a day in 2010; red indicates when sublimation exceeds deposition

Without understanding why these peaks appear, it was not possible to fit any parameterisation to explain the observed albedo variation for the clear afternoons, and thus only mean values could be used for each of the three snow conditions (Table 3).

Table 3: Mean albedo values used in the parameterisation for clear afternoons

Snow Condition	Mean α
Wet	0.74
Aged	0.80
Refrozen	0.82

4.4.3 Combining the Clear and Cloudy Skies

Thus far, this chapter has established rules for wet, aged and refrozen snow under 100% clear and 100% cloudy skies. To account for skies with a cloud cover between these two extremes, both the clear sky and cloudy sky albedo are calculated for the given hour, and a linear scaling is used to weight the contribution from each to the final albedo value.

For example, a SATR value of 0.9413 is 25% of the way between the clear (SATR = 0.914) and cloudy (SATR = 0.996) thresholds, and thus the final albedo would be calculated by summing 75% of the clear sky albedo value and 25% of the cloudy sky albedo value.

4.5 Final Rules of the Parameterisation

The albedo (α) for any hour can be calculated as:

$$\alpha = \alpha_{clear} * k_{clear} + \alpha_{cloud} * k_{cloud} \tag{16}$$

where the coefficients, k_{clear} and k_{cloud} are determined using the Sky Air Temperature Ratio (*satr*):

$$k_{cloud} = \frac{satr - 0.914}{0.996 - 0.914} \qquad \begin{matrix} if\ k_{cloud} > 1 & k_{cloud} = 1 \\ if\ k_{cloud} < 0 & k_{cloud} = 0 \end{matrix}$$

$$k_{clear} = 1 - k_{cloud}$$

The clear and cloudy sky albedo values (α_{clear} and α_{cloud}, respectively) are determined from the following tables:

$\boldsymbol{\alpha_{cloud}}$

Aged Snow	$\alpha_{cloud} = 0.86$
Refrozen Snow	$\alpha_{cloud} = 0.911 - 0.0644d$
Wet Snow	$\alpha_{cloud} = 0.902 - 0.0867d - 9.05lwc$

$\boldsymbol{\alpha_{clear}}$

	Morning	*Afternoon*
Aged Snow	$\alpha_{clear} = 1.27 - \frac{2}{3}\cos(90° - z)$	$\alpha_{clear} = 0.80$
Refrozen Snow	$\alpha_{clear} = 0.97 - 0.0644d - \frac{1}{3}\cos(90° - z)$	$\alpha_{clear} = 0.82$
Wet Snow	$\alpha_{clear} = 0.67$	$\alpha_{clear} = 0.74$

where *z* is the Solar Zenith Angle in degrees, *d* is the snow grain size in mm, and *lwc* is the liquid water content in m w.e.

5 Results

This chapter presents comparisons between the parameterisation and the albedo observed at KAN_U. It is restricted to displaying figures and provides only brief comments: attempts to explain the successes and failures of the scheme are provided in Chapter 6.

5.1 Entire Dataset

Figure 30 presents a comparison between the modelled and observed albedo using hourly values for the entire 8 year dataset (R^2 = 0.468; RMSE = 0.062, p = 0).

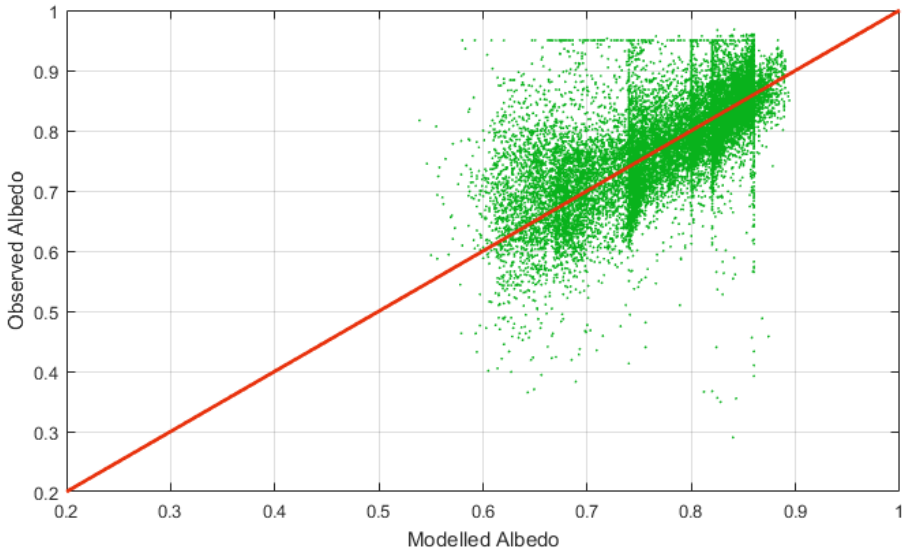

Figure 30: Comparison between observed and modelled hourly albedo over the entire dataset. The red line indicates a perfect match between the two.

There are clear stripes in the data that come from the rules which use mean values. It is also evident that the observed albedo can be higher than α = 0.90, whereas the modelled albedo cannot; similarly, there are examples of the observed albedo being lower than α = 0.50, whilst the minimum predicted by the model is α = 0.54.

Figure 31 reveals an approximately normal distribution in the residuals, with a marginal tendency to underestimate (47%) rather than overestimate (45%) the observed albedo. When compared at 2 decimal places, 8% of the values match exactly. Slightly more than 65% of the errors are within ± 0.05 of the observations, and 91% are within ± 0.1.

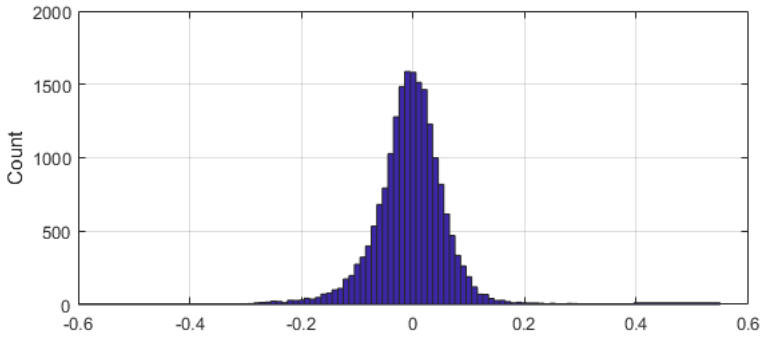

Figure 31: Histogram of the residuals. Negative values are underestimates

5.2 Annual Differences

Repeating the scatter plot for each year reveals large inter-annual differences (Figure 32). For example, the fit in 2009 (R^2 = 0.644) is over twice as successful as the fit in 2014 (R^2 = 0.287).

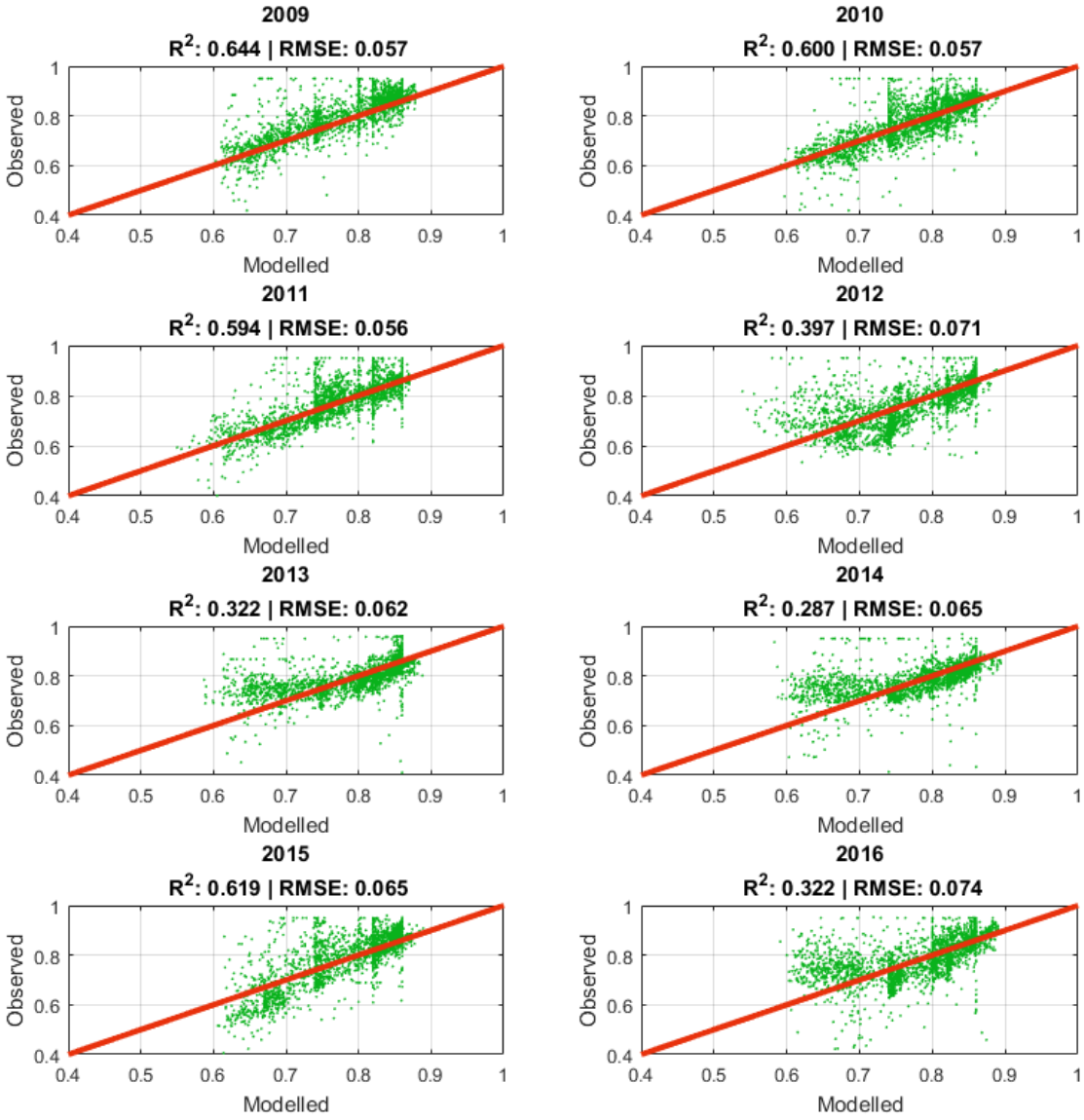

Figure 32: Annual scatter plots of modelled and observed albedo

The scheme can explain approximately 60% of the observed albedo for 2009, 2010, 2011, and 2015. In the remaining years, approximately 30-40% of the variation is captured.

Figure 33 indicates that the scheme tends to underestimate rather overestimate the albedo in 2009 and 2015, whilst the opposite is true in 2012 and 2014. The approximately normal distribution of residuals seen over the entire dataset (Figure 31) breaks down somewhat within individual years. For example, in 2013 and 2014 there are longer tails on the negative side, showing a wide spread of underestimates, whereas the majority of overestimates are still very close to 0. This is discussed in Chapter 6.

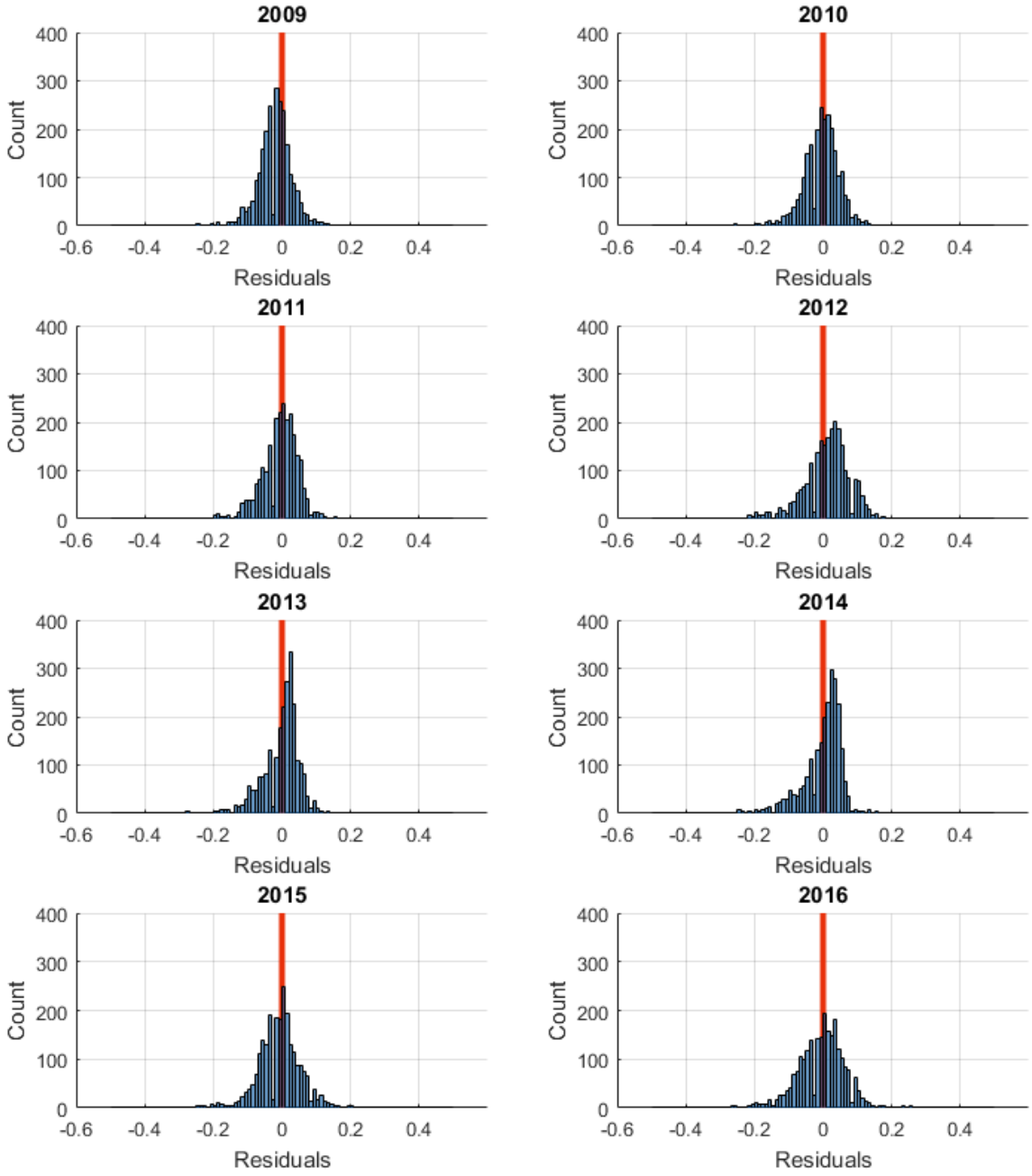

Figure 33: Histograms of the residuals for each year
Negative values indicate that the modelled albedo is too low, and positive too high

5.3 Monthly Differences

There is less variation between months than there is between years (Figure 34). However, the fit for October is noticeably poor, which could be because all values recorded in October occur at SZAs greater than 70°. Observing the scatter plots shows that many of the highest observed albedos (α=0.95) occur in May, whilst the fit otherwise looks to be very similar to June.

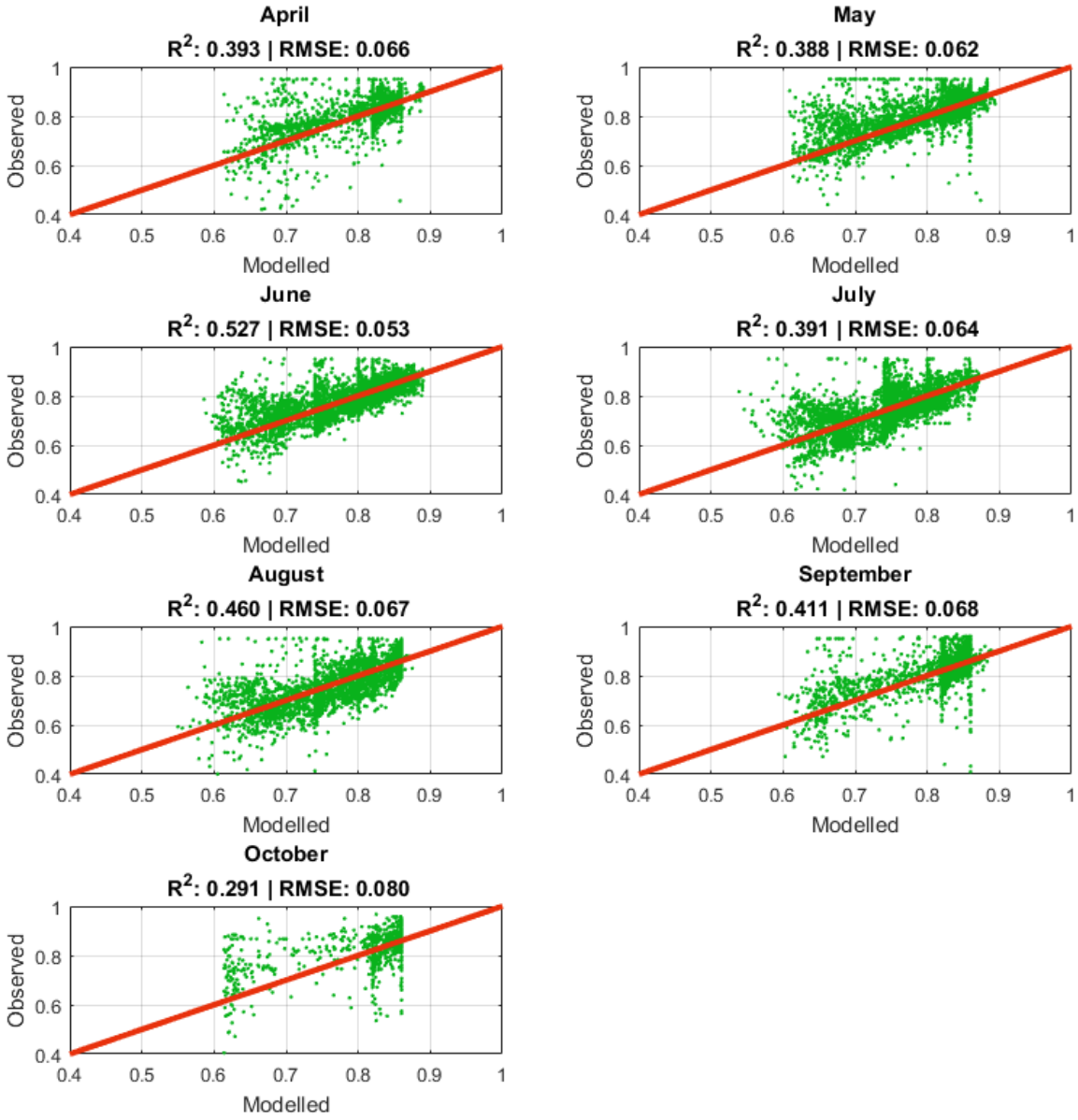

Figure 34: Monthly scatter plots of modelled and observed albedo

5.4 Snow Conditions Differences

The parameterisation worked almost equally well for each of the three snow conditions (Figure 35). The R^2 value was the highest for the refrozen snow albedo (R^2=0.489), but this also produced a larger RMSE value than for either the wet or aged snow.

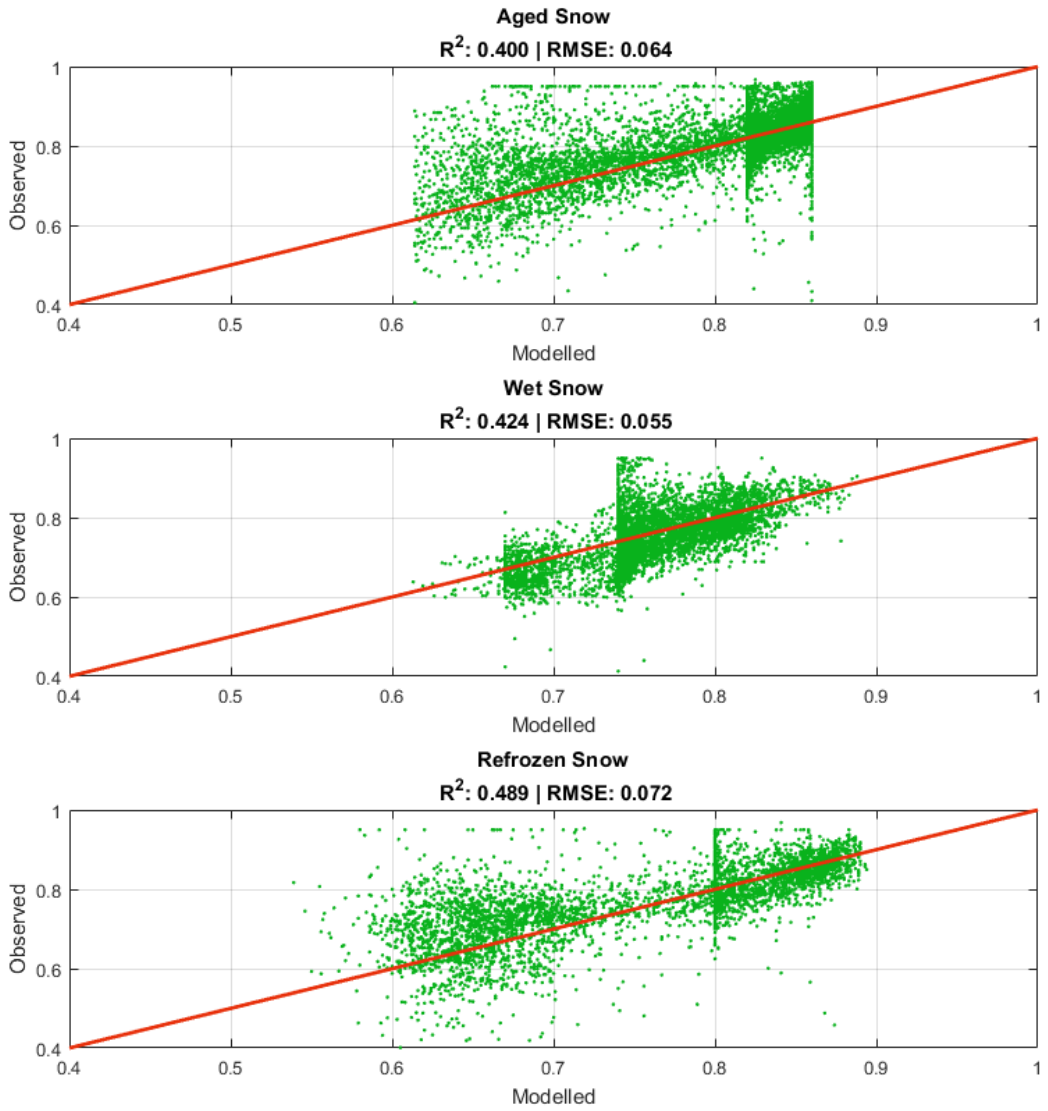

Figure 35: Scatter plots of observed and modelled albedo for each of the three snow conditions

In the refrozen snow, there is a clear separation in the albedo values that the model predicts, with very few in the range from α=0.70 to α=0.80. It is possible that the values have been systematically underestimated, as the left-hand side of the cloud would appear to fit better if it was around 0.05 to 0.1 higher.

5.5 Clear Skies & Cloudy Skies

Figure 36 shows differences between hours under different clear and cloudy sky conditions. Hours which are 100% cloudy produce a slightly better fit than those which are 100% clear. Hours when the sky is 75-100% cloudy are better represented than those which are 75-100% clear. This could potentially indicate that the contribution from the clouds is too strong for these values, suggesting that either the threshold used to define a clear sky is too low or that the choice of a linear scaling was not suitable.

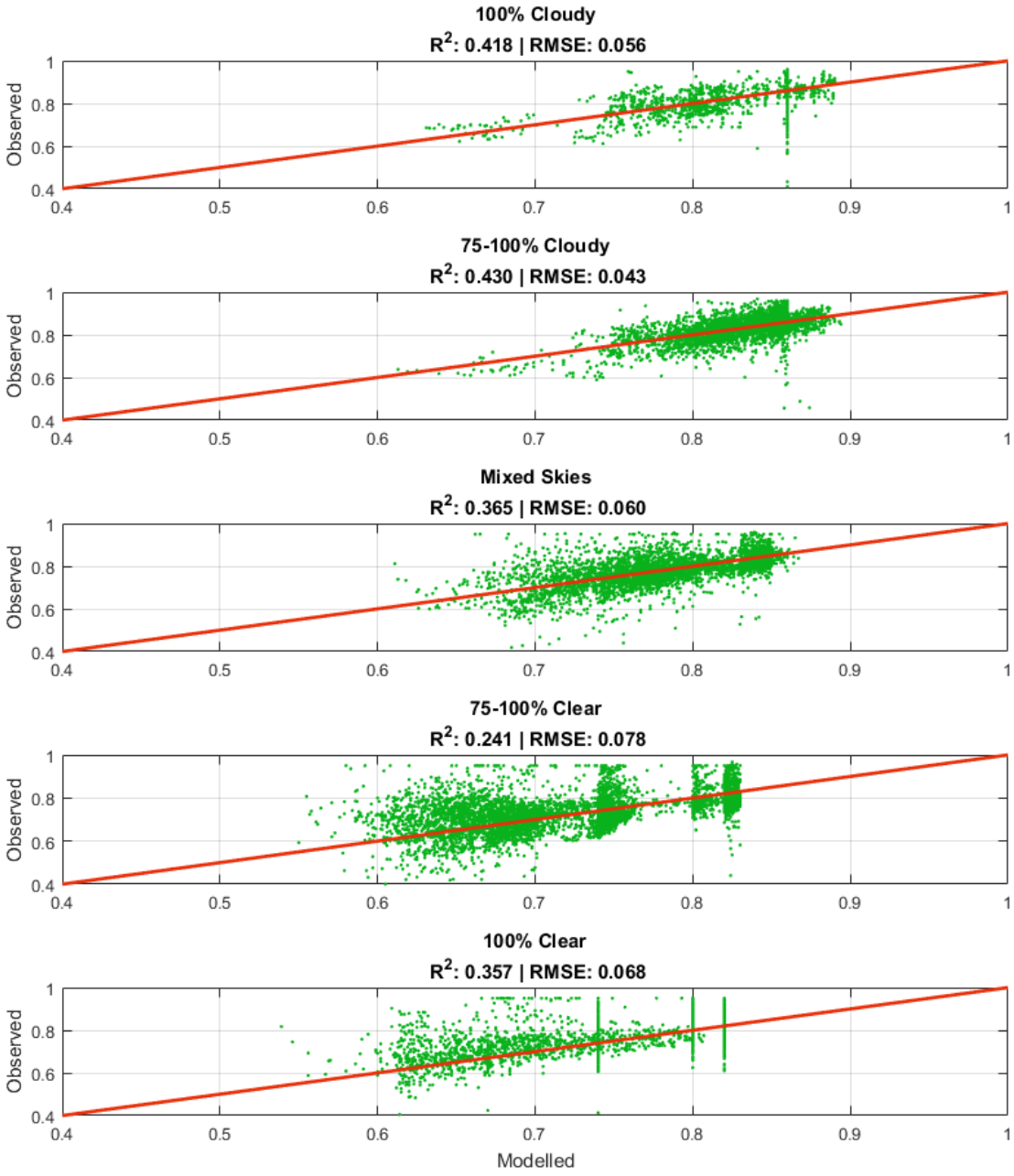

Figure 36: Scatter plots of observed and modelled albedo for five different cloud cover conditions. Cloudiness percentages are based on the linear SATR scaling used by the scheme

5.6 Examining Diurnal Patterns

Figure 37 presents 10 randomly-selected days from each year to show how well the parameterisation mimics the observed diurnal pattern. These plots show that there are occasionally time when the scheme is clearly incorrect, but much of the variation matches overall. In some instances, the pattern is well-replicated but offset by ~0.05 to 0.1 throughout the day; equally, there are days when the model approximates the mean value well, but doesn't capture the hourly variation.

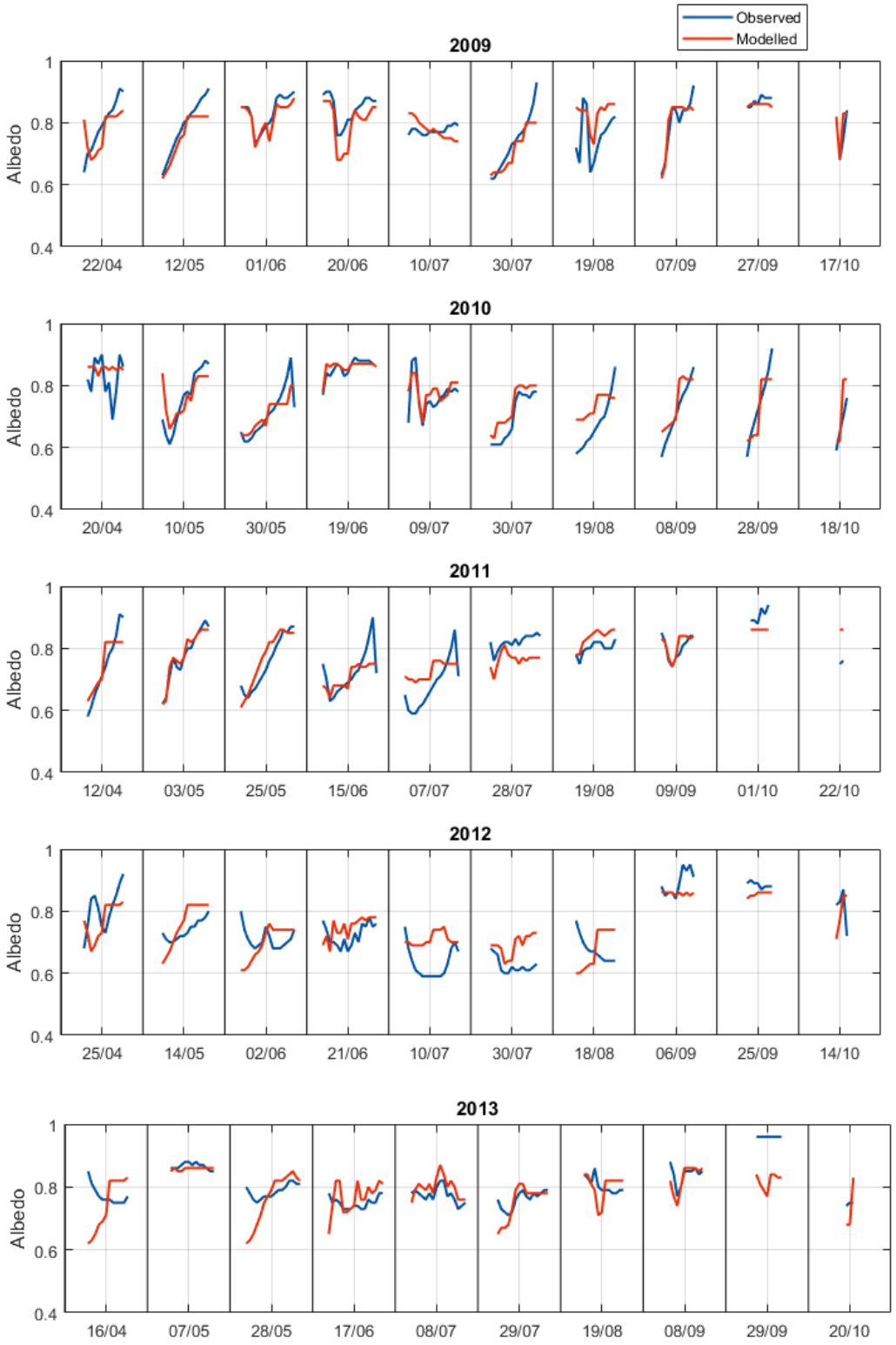

Figure 37: Comparing diurnal patterns for 10 random days each year
Values are plotted against the local time for each date shown on the x-axis; the faint grey line represents noon. Only hours when the SZA was less than 80° are plotted, explaining why the October days are so short.
Continues overleaf.

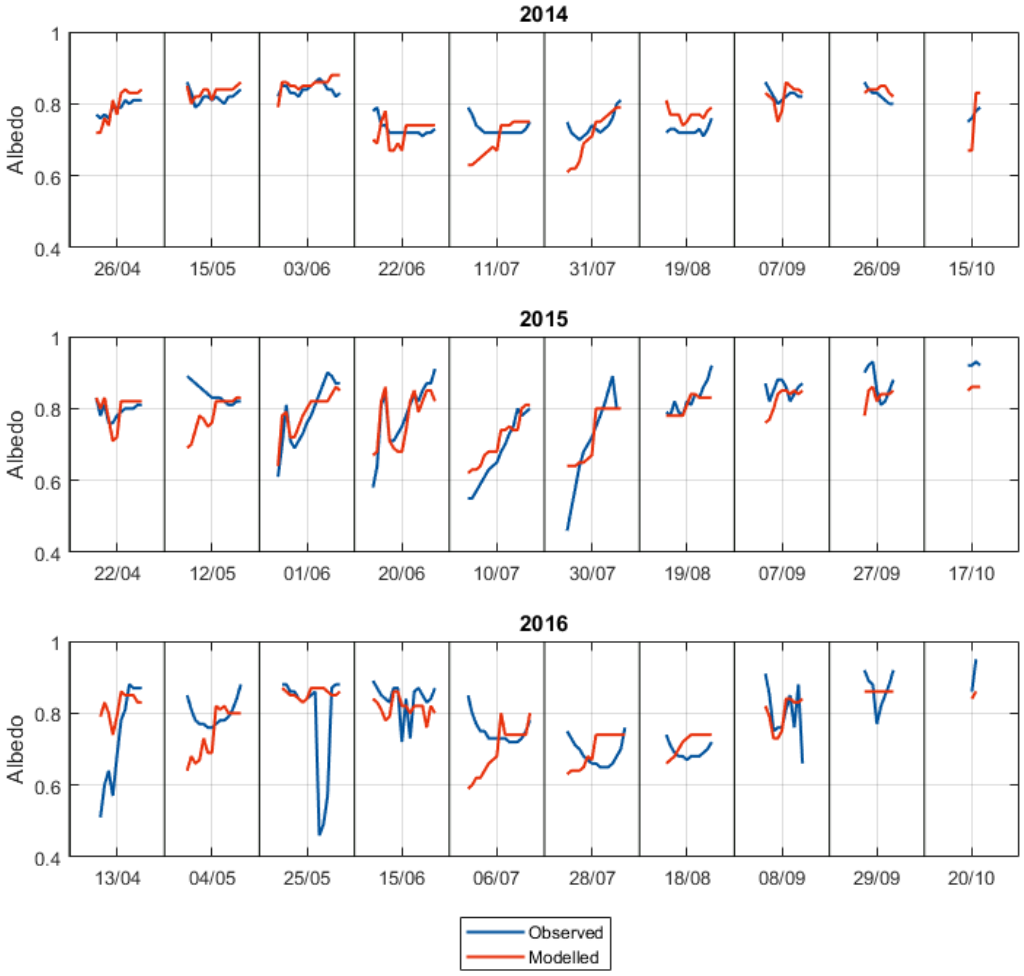

Figure 37 continued

6 Discussion

6.1 Overview of the Approach

The approach used in this thesis was to separate the snow into one of three conditions (aged, wet or refrozen) and create a rule for the clear sky and cloudy sky albedo value for each of these. It was expected that there would a definable relationship with the grain size for the cloudy sky albedo, which could then be modified with a term for the SZA to explain the diurnal variation of the clear sky albedo.

For the cloudy skies, understandable relationships were uncovered with the grain size for the refrozen snow albedo, and with the grain size and LWC for the wet snow albedo. However, no relationship was found for the dry snow albedo, and thus a mean value was used. Nevertheless, separating the data into different snow conditions produced a final R^2 fit of 0.425 for skies more than 75% cloudy (RMSE = 0.047).

In contrast, the clear skies presented numerous problems that complicated the approach. Initially, the unexpected increase in the albedo throughout the day meant that the cosine functions of SZA used by previous authors would not be applicable to this dataset. However, because these days had already been defined as only having clear skies, the SZA was left as the only possible variable that could change so much throughout a single day. It was therefore decided that the patterns should be described as a function of the SZA, making it necessary to handle the mornings and afternoons separately. Without a reason for why this would be the case, the scheme immediately becomes more specific to this dataset.

For the clear mornings, SZA functions were used for refrozen and aged snow albedo, but not for the wet snow albedo, which only had limited data. Clear afternoons contained unexplainable peak albedo values above SZAs of ~65°, which made it unreasonable to fit functions to the data without understanding if or when the peaks would occur.

Because of these decisions, the number of rules used by the parameterisation increased from six to nine, and five of them were mean values. This is potentially a major restriction of the scheme as it is possible that these values would need to be tuned with observations before it could be used in an alternative location. However, the separation between snow conditions provides a straightforward method of accounting for changes in the snowpack.

6.2 Decisions

6.2.1 Cloud Thresholds

To define the cloudy sky albedo, it was necessary to define a cloudy sky. This was the initial step used because it isolates the relationship between the albedo and the grain size.

The definition of a cloudy sky was based on the premise that albedo's dependence on the grain size would be at a maximum, and the relationship with the SZA at minimum. This is somewhat of a circular definition when building a rule for the albedo's relationship with grain size, but is physically understandable from the literature.

Initially, the SATR threshold was set using the median value (SATR = 0.986) identified from the boxplot, but this was found to be too low. For example, the relationship between the refrozen snow albedo and the grain size had a fit of R^2 = 0.08, and would therefore have been considered too low to base a rule for the parameterisation on. Increasing the threshold to 0.996 nearly doubled this (R^2= 0.15), and thus a rule based on the grain size was implemented.

This approach also necessitates that the cloud cover be considered equivalent. In reality, there will still be albedo variation owing to the cloudiness, particularly as the SATR used here does not account for the actual distribution of the cloud cover for example. It was decided the best way to account for these changes was

to use the highest possible SATR threshold for clouds, whilst still including enough data to analyse and create statistically significant rules from.

For the clear skies, the approach was more complicated because of the linearly rising albedo. This negated most of the relationships with the SZA as the high albedo value recorded in the afternoon opposed the low albedo value recorded in the morning at the same SZA. It was decided to use the median value from the SATR boxplot (SATR = 0.914) to define the clear skies. Attempts to lower this threshold left only a couple of days which would have been considered clear and therefore any rules based on them would have been difficult to justify.

It is evident that these thresholds have a very direct consequence on the rules formed for the parameterisation, and they are also used as the upper and lower bounds of the linear scaling in the final albedo calculation. Because of this importance, future work should look to verify these thresholds, and also see if they are consistent with other locations.

6.2.2 Sublimation & Deposition

Throughout the analysis, there were frequent relationships identified between the albedo and sublimation/deposition. These were not expected from the literature, and appear to be counterintuitive: they suggested that lower amounts of deposition and even sublimation would produce a higher albedo. It would be more logical to expect albedo to rise if more fine ice crystals are deposited at the surface, and for the sublimating conditions to lead to rounder grains and a lower albedo.

The sublimation variable is an output of the firn model, and can be considered a composite variable that is impacted by the temperature, humidity and wind speed for example. It is unclear exactly how this output would be replicated at the snow surface, particularly in relation to the albedo, and therefore sublimation was excluded from the analysis. It should be further investigated whether this relationship is found at other PROMICE sites.

6.2.3 SZA

Because the PROMICE data was an hourly average, it was decided to use a midpoint of the hour as the SZA value. However, this could lead to errors in the SZA as such a simple approximation may not be representative of the actual sun position for that hour (Blanc & Wald, 2016). This could lead to weaker-than-expected correlations with the SZA, and it would therefore be of interest to repeat the SZA analyses for the clear morning albedo using a more representative SZA. This may also be able to provide a clearer indication of whether the peaks observed on the clear afternoons are related to the SZA.

6.2.4 Snow Conditions

It was expected that designating each albedo value as either wet, refrozen or aged snow would be able to show the impacts of the dry and wet snow metamorphism, and refreezing. This was successful to a certain extent as the relationship between albedo and the grain size was only apparent after LWC had been present, but it is possible that the distinctions made here are too simple.

One potential problem is that the definition of refrozen snow is a binary choice based on a threshold of LWC = 0. Whilst the rapid effects of LWC on snow grain metamorphism are clear from the literature, such a distinction may over-simplify the difference between aged and refrozen snow albedo. This could, for example, make a big difference to the scheme in 2016, when a very early melt event was recorded, and the surface was subsequently classified as being refrozen for much of the year. It is perhaps not reasonable to expect this to behave in the same way as the refrozen snow that followed the large melt events of 2012.

Similarly, the surface was judged to have had aged snow if any snowfall had accumulated but not become wet. It may have been more appropriate to have set a minimum threshold, as the refrozen snow beneath a thin layer of new snow will still affect the surface albedo.

6.2.5 Specificity

As this thesis was undertaken, it was possible to create rules that were more detailed and precise than those that were used in the final scheme, which relied on a number of mean values. Whilst these means appear to describe much of the basic variation in albedo, the remaining errors highlight that there is still much that cannot be satisfactorily explained with this approach.

The reason that mean values were used instead of incorporating the more precise fits was because the division of the data had become incredibly specific. For example, a relationship with the SZA was discovered for refrozen snow when the sky was clear, but only for hours in the afternoon when the SZA was less than 65°. Whilst a relationship with the SZA could be expected for this, it was decided such divisions were highly prescriptive for certain subsets of the data, and the different coefficients or forms that the functions took could not be explained.

In the final scheme, only two separate SZA functions were used. These were for aged and refrozen snow on clear mornings. Although it is still specific to separate these, there was a clear difference in the gradient of their diurnal patterns when plotted as a function of SZA (Figure 24 and Figure 26). It is possible that the shallower gradient of the refrozen snow albedo can be understood as a result of the grain rounding that occurred when the snow was wet, losing any preferential scattering directions and reducing the amount of difference that the SZA makes (Painter & Dozier, 2004).

6.3 Inter-Annual Differences

The success of the scheme varied between years, producing stronger fits in 2009-2011 and 2015 than in 2012-2014 and 2016. Examining the distribution of the observed albedo for each year (Figure 38) shows that 2013 and 2014 have a clear minimum albedo: for example, in 2014, there are only 77 hours with an albedo lower than $\alpha = 0.69$, and in 2013 only 104 hours; in all other years, there are at least 300 hours with these very low albedo values.

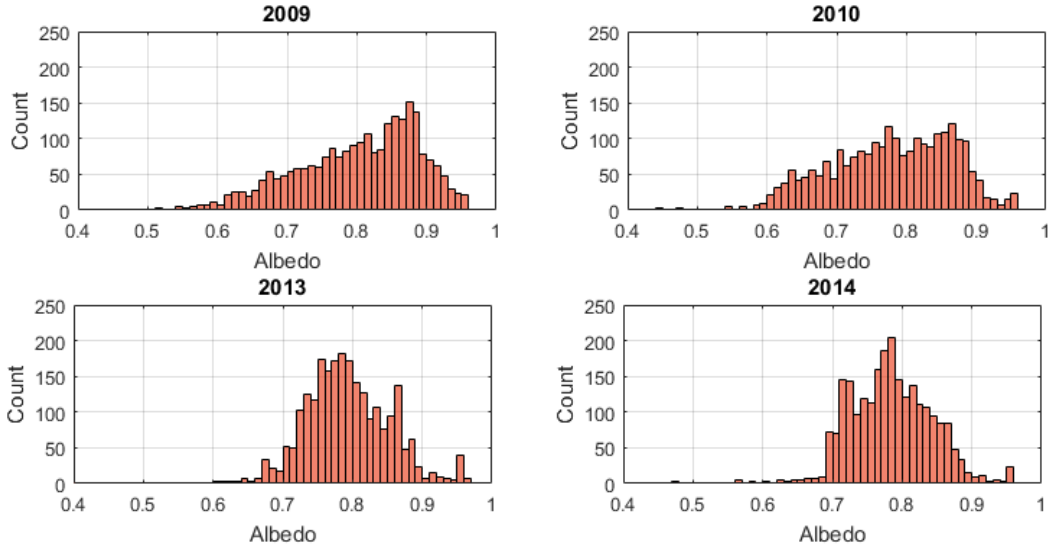

Figure 38: Distributions of the observed albedo for selected years.
Only the dataset used in the parameterisation is plotted (i.e. hours in summer with SZA <80° and at least 50W/m^2 of incoming shortwave radiation)

It appears that the differences in the observed albedo distribution could explain why 2013 and 2014 have lower R^2 fits than the other years. Repeating Figure 38 with the distribution of the modelled albedo shows that the predictions are very similar for 2010 and 2014 (Figure 39). This suggests that the model encountered very similar conditions in these two years, in terms of the cloudiness and snow conditions, and the poor fit is therefore because the rules used in the scheme do not apply as well to 2014 as they do to 2009.

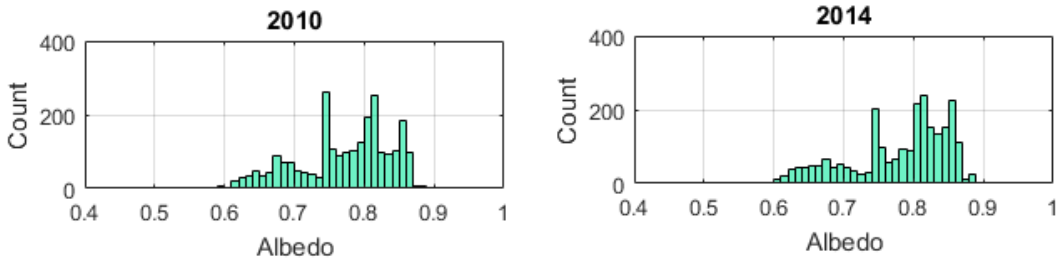

Figure 39: Modelled albedo distribution

It is not clear why this would be. One potential explanation could relate to when the snow conditions appear (Figure 40). For example, in 2010, there is a much longer period when the snow is wet, and this could allow the albedo to continue falling further due to the surface-albedo feedback. In 2014, this feedback would be interrupted more often because there are three distinct periods of refrozen snow, and therefore the albedo may not continue falling until the lowest values. However, this would not explain the difference between 2014 and the other years, and is only proffered as a potential idea.

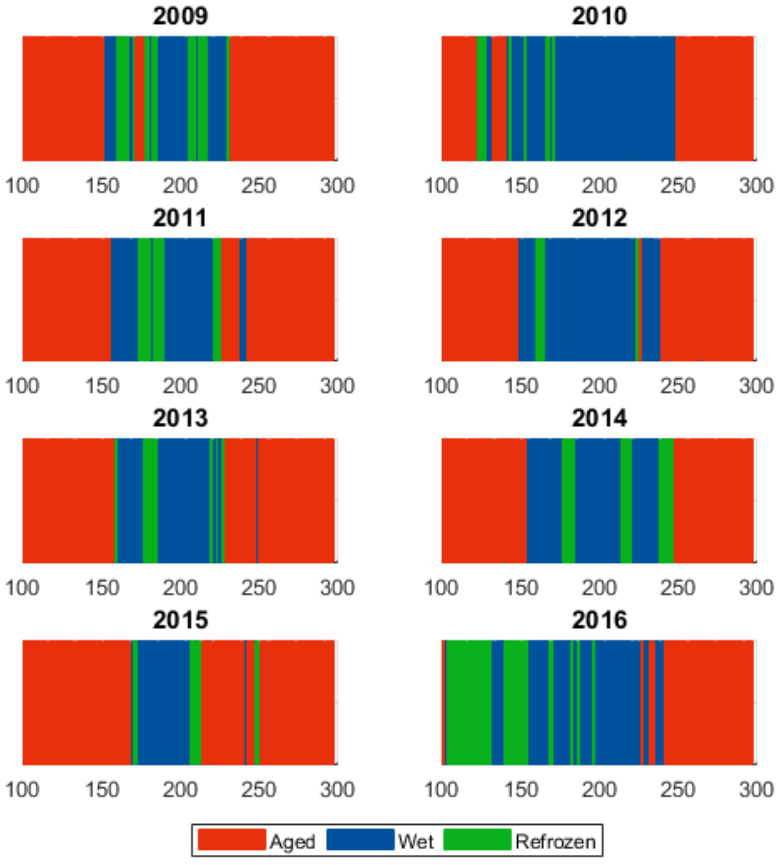

Figure 40: Snow conditions for each year
Values on the x-axis are the day of the year

One other possibility is that the extensive melt seen in 2012 could relate to the scheme's worsening fit, although it is unclear how this would be the case. For example, Box et al. (2012) point out a low albedo and strong melt can precondition the ice sheet for the next year, but this would be expected to increase the number of hours with a low albedo, rather than defining a new, higher minimum albedo value. Further works needs to understand why the observed albedo changed between years, and to see if this can be incorporated into the parameterisation.

6.4 Additional Findings

6.4.1 Daily SATR & Albedo

The intention of this thesis was to parameterise the albedo on an hourly basis. However, clear relationships between the daily average SATR and daily average albedo were also discovered (Figure 41). These were particularly successful if the days were separated into wet snow and dry snow days.

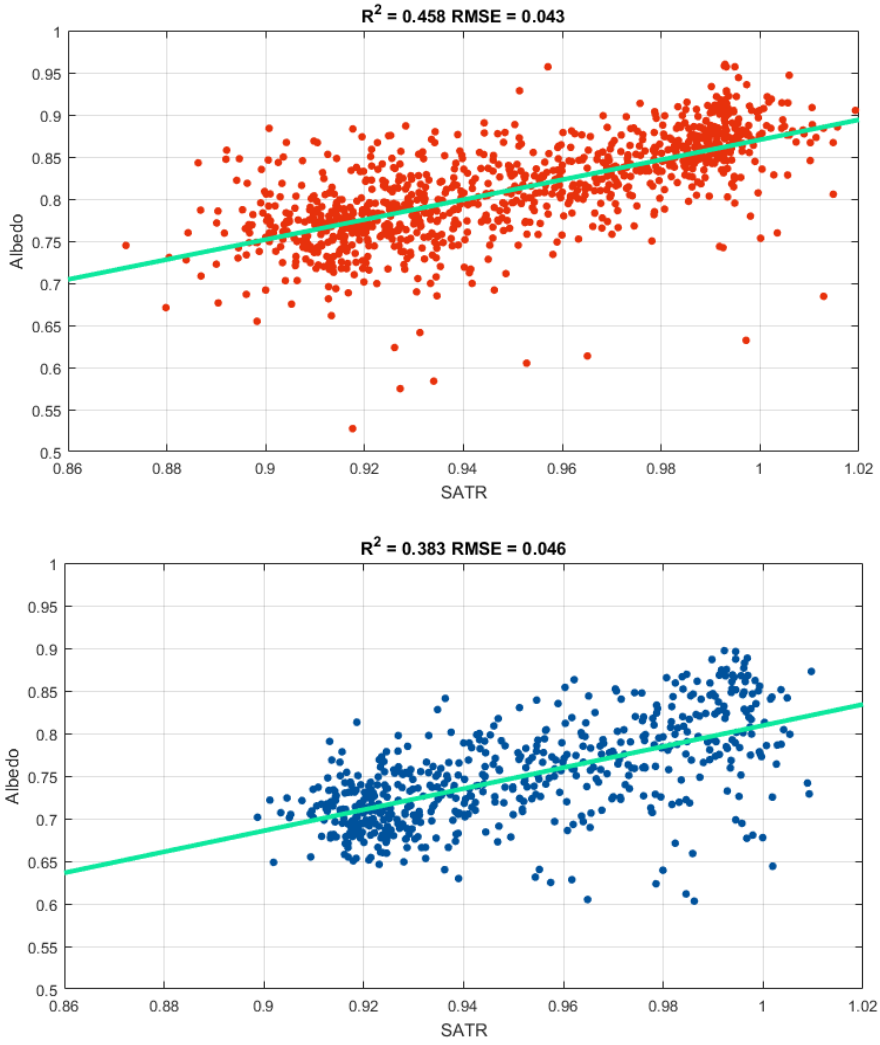

Figure 41: Daily average SATR and albedo for dry days (top) and wet days (bottom)

These plots also show a clear drop in the daily albedo from dry snow days to wet snow days: a linear fit through each dataset is almost identical but lower by ~0.07 for the wet days. This relationship is an

interesting finding, because it indicates that much of the albedo can be determined purely from the cloudiness of the sky, and a binary distinction of whether the snow is wet or not.

6.5 Recommendations & Further Work

6.5.1 Validation

The parameterisation created in this thesis was only compared against the data that it was created from. It is necessary to test this scheme at further PROMICE stations with their own in-situ albedo records, and evaluate how much of the variability can be captured with the current scheme. It is expected that the success of this will differ depending on the sites tested. For example, the scheme used here is based on KAN_U, which sits in the accumulation zone, and is always snow-covered: many of the other PROMICE stations are located in the ablation zone, where bare ice is often revealed, and thus the current scheme would need to be modified to incorporate the snow depth, and ice albedo. However, a more immediate issue with the scheme may be that it replicates the unexpected albedo rise in the morning, rather than falling as is expected. It is unclear whether this is unique to KAN_U, or would be encountered at other stations.

It is also necessary to compare how well this scheme performs at KAN_U with other albedo schemes. For example, the scheme of Nielsen-Englyst (2015) is a time-dependent scheme that has been used in the HIRHAM5 regional climate model. Comparisons against schemes such as this are necessary to evaluate whether the current parameterisation provides any improvements, and if so, how reliably and by how much.

6.5.2 Snow Grain Size

For wet and refrozen snow, relationships were found between albedo and the modelled grain size, whereas this was not the case for the dry, aged snow. This could indicate that the firn model is better able to replicate grain growth associated with melt metamorphism than it is for isothermal or temperature gradient metamorphism. It is suggested that the model could potentially be expanded to include a different way of replicating dry snow metamorphism.

7 Conclusions

This thesis has created a new parameterisation for snow albedo using output from a firn evolution model to explain 8 years of albedo observations at the KAN_U PROMICE weather station. The scheme differentiates between three snow conditions (aged, refrozen, and wet), and uses four variables as inputs: the Solar Zenith Angle (SZA); the Sky-Air Temperature Ratio (SATR); the Liquid Water Content (LWC); and the modelled grain size. Clear and cloudy sky albedo values are calculated for each time-step and a linear scaling based on the SATR determines their relative contributions to the final albedo value. The scheme is applicable in the summer (days 100-300) for hours with a SZA <80° and at least 50W/m^2 of incoming shortwave radiation.

The success of the scheme varies between years: in the initial three years (2009-2011), overall fits of R^2 > 0.6 are produced, but the following three years are clearly worse, falling to a minimum fit of R^2 = 0.287 in 2014. The scheme again captures much more of the variability in 2015, before finally performing poorly in 2016. Compared to the other years, 2013 and 2014 have very few hours with $\alpha < 0.69$, yet the model predicts a similar albedo distribution for these years as it does for 2009 and 2010, when the scheme is judged more successful. It is not clear why the observed albedo and therefore the fit of the scheme differs so much between these years, but the extensive melt in 2012 is tentatively suggested as a possible contributing factor that should be explored further.

This scheme has only been validated against the observed albedo from KAN_U: it is a priority to test the scheme with albedo observations from other PROMICE stations. One potential problem with applying this scheme to other sites is that it specifically predicts the albedo to rise from the early morning to noon. This was apparent from the observations at KAN_U, but contradicts theory, and therefore it remains to be seen whether this is replicated elsewhere. Nevertheless, it is suggested that the approach taken here to make a simple distinction between the snow conditions and the cloud conditions could be used as a basis for other locations with relatively straightforward modifications to the exact rules of the parameterisation. However, it is first necessary to compare the success of this scheme against other schemes when using the same input data.

Relationships between the albedo and grain size were found for the refrozen and wet snow, but not for the aged snow. This could potentially suggest that the firn model may simulate melt metamorphism better than temperature-gradient or isothermal metamorphism. It is also clear that the LWC is important for wet snow albedo.

Aside from the parameterisation, the albedo observations at KAN_U revealed three characteristic features: (1) the diurnal pattern for clear skies was not the theorised smile, but rather an approximately linear rise throughout the day; (2) there were peak albedo values in the late afternoon that were unable to be correlated with any meteorological variables and remain unexplained; and (3) approximately 1/3 of the variation in daily averaged albedo can be described as a linear function of the daily averaged SATR, with even better fits achievable if a simple distinction is made between wet snow and dry snow days.

8 References

Ahlstrøm, A.P., Gravesen, P., Andersen, S., Van As, D., Citterio, M., Fausto, R., Nielsen, S., Jepsen, H.F., Kristensen, S.S., Christensen, E.L., Stenseng, L., Forsberg, R., Hanson, S. & Petersen, D. (2008) A new programme for monitoring the mass loss of the Greenland ice sheet. *Geological Survey of Denmark and Greenland Bulletin,* 15, 61-64. [Available online at: http://www.geus.dk/DK/publications/geol-survey-dk-gl-bull/15/Documents/nr15_p61-64.pdf]

Aoki, T., Aoki, T. & Fukabori, M. (2000) Effects of snow physical parameters on spectral albedo and bidirectional reflectance of snow surface. *Journal of geophysical Research,* 105, D8, 10,219-10,236.

Arons, E.M. & Colbeck,S.C. (1995) geometry of heat and mass transfer in dry snow: A review of theory and experiment. *Reviews of Geophysics*, 33, 4, 463 – 493.

Bader, H. (1939) Mineralogical and structural characterization of snow and its metamorphism in H. Bader, R. Haefeli, E. Buchker, J. Neher, O. Eckel, & C. Thams. Snow and Its Metamorphism, Beiträge zür Geologie der Schweiz, Geotechnische Serie, Hydrologie, Bern, p. 1–55.

Barry, R.G (1996) The parameterization of surface albedo for sea ice and its snow cover. *Progress in Physical Geography*, 20, 1, 63 – 79.

Blanc, P. & Wald, L. (2016) On the effective solar zenith and azimuth angles to use with measurements of hourly irradiation. *Advances in Science and Research,* 1, 1-6, doi:10.5194/ars-1-1-2016.

Bohren, C.F. & Barkstrom, B.R. (1974) Theory of optical properties of snow. *Journal of Geophysical Research*, 79, 30, 4527-4535.

Bohren, C.F. & Beschta, R.L. (1979) Snowpack albedo and snow density. *Cold regions and Technology*, 1, 47-50.

Bond et al., 2013; Bond, T.C., Doherty, S.J., Fahey, D.W., Forster, P.M., Bernsten, T., DeAngelo, .J., Flanner, M.G., Ghan, S., Kärcher, B., Koch, D. Kinne, S., Kondo, Y., Quinn, P.K., Sarofim, M.C., Schultz, M.G, Venataraman, C., Zhang, H., Zhang, S., Bellouin, N., Guttikunda, S.K., Hopke, P.K., Jacobson, M.Z., Kaiser, J.W., Klimont, Z., Lohmann, U., Schwarz, J.P., Shindell, D., Storelvmo, T., Warren, S.G. & Zender, C.S. (2013) Bounding the role of black carbon in the climate system: A scientific assessment. *Journal of Geophysical Research: Atmospheres,* 188, 5380-5552.

Bougamont, M., Bamber, J.L. & Greuell, W. (2005) A surface mass balance model the Greenland Ice Sheet. *Journal of Geophysical Research*, 110*,* F04018.

Box, J. E., Fettweis, X., Stroeve, J. C., Tedesco, M., Hall, D. K., & Steffen, K. (2012) Greenland ice sheet albedo feedback: thermodynamics and atmospheric drivers. *The Cryosphere*, 6, 821-839

Brock, B.W., Willis, I.C. & Sharp, M.J. (2000) Measurement and parameterization of albedo variations at Haut Glacier d'Arolla, Switzerland. *Journal of Glaciology,* 46, 155, 675 – 688.

Brun, E. (1989) Investigations on wet-snow metamorphism in respect of liquid water content. *Annals of Glaciology,* 13, 22 – 26.

Brun, E., David, P., Sudul, M. & Brunot, G. (1992) A numerical model to simulate snow-cover stratigraphy for operational avalanche forecasting. *Journal of glaciology,* 38, 128, 13-22.

Charalampidis, C., Van As, D., Box, J.E., Van Den Broeke, M.R., Colgan, W. T., Doyle, S.H., Hubbard, A.L., MacFerrin, M., Machguth, H. & Smeets, C.J.P.P. (2015) Changing surface-atmosphere energy exchange and refreezing capacity of the lower accumulation area, West Greenland. *The Cryosphere*, 9, (6), 2163-2181. doi: 10.5194/tc-9-2163-2015

Chylek, P., Ramaswamy, V. & Srivastava, V. (1983) Albedo of Soot-Contaminated Snow. *Journal of Geophysical Research,* 88, C15, 10,837-10,843.

Colbeck, S. (1975) A theory of water flow through a layered snowpack. *Water Resources Research*, 11, 2, 261-266.

Colbeck, S. C. (1979) Grain clusters in wet snow. *Journal of Colloid & Interface Sciences,* 72, 371–384.

Colbeck, S. C. (1980) Thermodynamics of snow metamorphism due to variations in curvature. *Journal of Glaciology,* 26, 94, 291–301.

Colbeck, S. (1983) Theory of metamorphism of dry snow. *Journal of Geophysical Research,* 88, C9, 5475-5482.

Coleou, C. & Lesaffre, B. (1998) Irreducible water saturation in snow: experimental results in a cold laboratory. *Annals of Glaciology*, 26, 64–68.

Collins, W.D., Bitz, C., Boville, B.A., Briegleb, B., Dai, Y., Hack, J.J., Kiehl, J.T. , Lin, S.-J. , Macaa, J.R., Rasch, P. J., Rood, R. B., Williamson, D. L. & Zhang, M. (2002) Description of the NCAR Community Atmosphere Model (CAM2). [Accessible online @ http://www.ccsm.ucar.edu/models/atm-cam/docs/cam2.0/description/index.html]

Cook, J.M., Hodson, A.J., Gardner, A.S., Flanner, M., Tedstone, A.J., Williamson, C., Irvine-Flynn, T.D.L., Nilsson, J., Bryant, R. & Tranter, M. (2017) Quantifying bio albedo: a new physically based model and discussion of empirical methods for characterizing biological influence on ice and snow albedo. *The Cryosphere*, 11, 2611-2621.

Cuffey, K.M. & Paterson, W.S.B. (2010) *The Physics of Glaciers*. 4th edition, Elsevier.

Dozier, J., Schneider, S-R- & McGinnis Jr, D.F. (1981) Effect of Grain Size and Snowpack Water Equivalence on Visible and Near-Infrared Satellite Observations of Snow. *Water Resources Research*, 17, 4, 1213-1221.

Dozier, J., Green, R.O., Noli, A.W., & Painter, T.H. (2009) Interpretation of snow properties from imaging spectrometry. *Remote Sensing of Environment,* 113, S25-S37.

Dozier, J. (1989) Spectral Signature of Alpine Snow Cover from the Landsat Thematic Mapper. *Remote Sensing of the Environment,* 28, 9 - 22

Essery, R., Morin, S., Lejeune, Y. & Ménard, C.B. (2013) A comparison of 1701 snow models using observations from an alpine site. *Advances in Water Resources,* 55, 131-148.

Ewert, H., A. Groh, and R. Dietrich (2012) Volume and mass changes of the Greenland ice sheet inferred from ICESat and GRACE. *Journal of Geodynamics*, 59, 111–123.

Flanner, M. G., & Zender, C.S. (2006) Linking snowpack microphysics and albedo evolution. *Journal of Geophysical Research*, 111, D12208

Flanner, M.G., Zender, C.S., Randerson, J.T. & Rasch, P.J. (2007) present-day climate forcing and response from black carbon. *Journal of Geophysical Research,* 112, D11202.

Fuji, Y., Kawahara, H., Suto, Y., Fujud, S., Nakajima, T., Livengood, T.A. & turner, E.L (2011) Colors of a second Earth II: Effects of cloud son photometric characterization of earth-like exoplanets. *The Astrophysical Journal,* 738, 184.

Gardner, A.S. & Sharp, M.J. (2010) A review of snow and ice albedo and the development of a new physically based broadband albedo parameterization. *Journal of Geophysical Research,* 115, F01009.

Gregory, J.M., Huybrechts, P. and Raper, S.C.B. (2004) Threatened loss of the Greenland ice-sheet. *Nature, 428, 616*.

Grenfell, T.C. & Maykut, G.A. (1977) The optical properties of ice and snow in the Arctic Basin. *Journal of Glaciology,* 18, 80, 445 – 463.

Grenfell, T.C. & Warren, S.G. (1999) Representation of a non-spherical ice particle by a collection of independent spheres for scattering and absorption of radiation. *Journal of Geophysical Research,* 104, D24, 31,697 – 31,709.

Grenfell, T.C., Neshyba, S.P. & Warren, S.G. (2005) Representation of a non-spherical ice particle by a collection of independent spheres for scattering and absorption of radiation: 3. Hollow columns and plates. *Journal of Geophysical Research: Atmospheres,* 110, D17.

Greuell, W. (2002) Melt-Water Accumulation on the Surface of the Greenland Ice Sheet: Effect on Albedo and Mass Balance. *Geografiska Annaler - Series A, Physical Geography*, 82, 4, 489-498.

Hall, A (2004) The role of surface albedo feedback in climate. *Journal of Climate*, 17, 7, 1550–1568

Hanna, E., et al. (2011) Greenland Ice Sheet surface mass balance 1870 to 2010 based on Twentieth Century Reanalysis, and links with global climate forcing. *J. Geophys. Res.*, 116, D24121.

Hansen, J. & Nazarenko, L. (2004) Soot climate forcing via snow and ice albedos. *PNAS*, 101, 2, 423-428.

Henderson-Sellers, A. & Wilson, M.F. (1983) Surface albedo data for climatic modelling. *Reviews of Geophysics and Space Physics,* 21, 8, 1743-1778.

Hubley, R.C. (1955) Measurements of Diurnal Variations in Snow Albedo on Lemon Creek Glacier, Alaska. *Journal of Glaciology,* 1955, 560-563.

Hudson, S.R., Warren, S.G., Brandt, R.E., Grenfell, T.C. & Six, D. (2006) Spectral bidirectional reflectance of Antarctic snow: measurements and parameterization. *Journal of Geophysical Research,* 111, D18106.

Jensen, H.W., Marschner, S.R., Levoy, M. & Hanrahan, P. (2001) A practical moel for subsurface light transport. *ACM SIGGRAPH 2001*, 12-17 August 2001.

Jordan, R. (1991) A one-dimensional temperature model for a snow cover: Technical documentation for SNTHERM 89, *Tech. Rep. Spec. Rep. 91-16*, U.S. Army Cold Regions Res. and Eng. Lab., Hanover, N. H.

Katsushima, T., Kumakura, T., and Takeuchi, Y. (2009) A multiple snow layer model including a parameterization of vertical water channel process in snowpack. *Cold Regions Science & Technology*, 59, 143–151. doi: 10.1016/j.coldregions.2009.09.002

Kiehl, J.T., Wolski, R.J., Briegleb, B. & Ramanathan, V. (1987): Documentation of radiation and cloud routines in the NCAR community climate model (CCMI). Report NCAR/TN-288+STR+ 1A. Boulder, CO: National Center for Atmospheric Research.

Kipp & Zonen (2018) CNR4 Net Radiometer Instruction Manual. [Available online at: www.kippzonen.com/Download/354/Manual-CNR-4-Net-Radiometer-English]

Klok, E.J. & Oerlemans, J. (2004) Modelled climate sensitivity of the mass balance of Morteratschgletscher and its dependence on albedo parameterization. *International Journal of Climatology*, 24, 231-245.

Kokhanovsky, A.A. & Zege, E.P. (2004) Scattering Optics of Snow. *Applied Optics,* 43, 7, 1589 -1602.

Kuipers Munneke et al. 2011

Journal of Geophysical research, Langen, P.L., Fausto, R.S., Vandecrux, B., Mottram R.H., & Box, J.E. (2017) Liquid Water Flow and Retention on the Greenland Ice Sheet in the Regional Climate Model HIRHAM5: Local and Large-Scale Impacts. *Frontiers in Earth Science*, 4:110, doi: 10.3389/feart.2016.00110

Langen, P.L., Mottram, R.H., Christensen, J.H., Boberg, F., Rodehacke, C.B., Stendel, M., Van As, D., Ahlstrøm, A.P., Mortensen, J., Rysgaard, S., Petersen, D., Svendsen, K.H., Aðalgeirdóttir, G. & Cappelen, J. (2015) Quantifying Energy and Mass Fluxes Controlling Gothåbsfjord Freshwater Input in a 5-km Simulation (1991-2012). *Journal of Climate,* 28: 3694-3713; doi: 10.1175/jcli-d-14-00271.1

Lefebre, F., Gallee, H., van Ypersele, J. P. & Greuell, W. 2003 Modeling of snow and ice melt at ETH Camp (west Greenland): A study of surface albedo. *Journal of Geophysical Research*, 108, D8, 4231.

Leroux, C., Deuze, J.L., Goloub, P., Sergent, C. & Fily, M. (1998) Ground measurements of the polarized bidirectional reflectance of snow in the NIR spectral domain - Comparisons with model results. *Journal of Geophysical Research,* 103, D16, 19721-19731.

Li, S. & Zhou, X. (2004) Modelling and measuring the spectral bidirectional-reflectance factor of snow–covered sea ice. An inter-comparison study. *Hydrological Processes,* 18, 3559-3581.

Manabe, S. & Stouffer, R.J. (1980) Sensitivity of a global climate model to an increase of CO2 concentration in the atmosphere. *Journal of Geophysical Research,* 85, C10, 5529-5554.

Neshyba, S.P., Grenfell, T.C. & Warren, S.G. (2003) Representation of a nonspherical ice particle by a collection of independent spheres for scattering and absorption of radiation - 2 - Hexagonal columns and plates. *Journal of Geophysical Research,* 108, D15, 4448.

Nghiem, S.V., Hall, D.K., Mote, T.L., Tedesco, M., Albert, M.R., Keegan, K., Shuman, C. DiGirolamo, N.E. & Neumann, G. (2012) The extreme melt across the Greenland ice sheet in 2012. *Geophysical Research Lett*ers, 39, 20, L20502.

Nielsen-Englyst, P. (2015) Impact of Albedo Parameterizations on Surface Mass Balance Runoff on the Greenland Ice Sheet. *Master Thesis, University of Copenhagen.*

NOAA (2018) NOAA Solar Calculator. *https://www.esrl.noaa.gov/gmd/grad/solcalc/*.

O'Brien, H. & Munis, R.H. (1975) Red and NIR spectral reflectance of snow. *Cold Regions Research and Engineering Laboratory,* Hanover, N.H.

Oerlemans, J., & Knap, W. H. (1998) A 1 year record of global radiation and albedo in the ablation zone of Morteratschgletscher, Switzerland. *Journal of Glaciology*, 44, 231–23.

Painter, T.H. & Dozier, J. (2004) Measurements of the hemispherical-directional reflectance of snow at fine spectral and angular resolution. *Journal of Geophysical Research,* 109, D18, D18115.

Petzold, D.E. (1977) An estimation technique for snow surface albedo. *Climatology Bulletin,* 21, 1-11.

Pirazzini, R. (2004) Surface albedo measurements over Antarctic sites in summer. *Journal of Geophysical Research,* 109, D20118, doi: 10.1029/2004JD004617.

Pirazzini, R. (2009) Challenges in snow and Ice albedo parameterizations. *Geophysica,* 45, 1-2, 41-62.

Reijmer, C.H., van Meijgaard, E. & can den Broeke, M.R. (2005) Evaluation of temperature and wind over Antarctica in a RCM using 1 year of AWS data and upper air observations. *Hournal of geophysical Resarch,* 110, D04103.

Roeckner, E., Bäuml, G., Bonaventura, L., Brokopf, R., Esch, M., Giorgetta, M., Hagemann, S., Kirchner, I., Kornblueh, L., Manzini, E., Rhodin, A., Schelse, U., Schulzweida, U. & Tompkins, A. (2003) The atmospheric

general circulation model ECHAM5. Part I: Model description. *Max Planck Institute for Meteorology Report*, 49, 140 pp. [Available online at http://www.mpimet.mpg.de/fileadmin/publikationen/Reports/max_scirep_349.pdf]

Roeckner, E., Arpe, K., Bengtsson, L., Christoph, M., Claussen, M., Dümenil, L., Esch, M., Giorgetta, M., Schlese, U. & Schulzweida, U., 1996. The atmospheric general circulation model ECHAM-4: model description and simulation of present-day climate. Max-Planck Institute for Meteorology Report, No. 218, Hamburg, Germany, 90pp.

Sasgen, I., et al. (2012) Timing and origin of recent regional ice-mass loss in Greenland. *Earth Planet. Sci. Lett*., 333, 293–303.

Schaepman-Strub, G., Schaepman, M.E., Painter, T.H., Dangel, S. & Martonchik, J.V. (2006) Reflectance quantities in optical remote sensing – definitions and case studies. *Remote Sensing of Environment,* 103, 27-42.

Segal, M., Garratt, J., Pielke, R. & Ye, Z. (1991) Scaling and numerical model evaluation of snow-cover effects on the generation and modification of daytime mesoscale circulations, *Journal of Atmospheric Sciences*, 48, 1024–1042.

Sellers, W.D. (1969) A global climatic model based on the energy balance of the earth-atmosphere system. *Journal of Applied Meteorology* 8, 392 – 400.

Shepherd, A., et al. (2012) A reconciled estimate of ice-sheet mass balance. *Science*, 338, 1183–1189.

Stanton, B., Miller, D., Adams, E. & Shaw, J.A. (2016) Bidirectional-reflectance measurements for various snow crystal morphologies. *Cold Regions Science & Technology,* 124, 110-117.

Stroeve, J., Box, J.E., Wang, Z., Schaaf, C. & Barrett, A. (2013) Re-evaluation of MODIS MCD43 Greenland albedo accuracy and trends. *Remote Sensing of Environment,* 138, 199 – 214.

Tedesco, M., Fettweis, X., van den Broeke, M. R., van de Wal, R. S. W., Smeets, C. J. P. P., van de Berg, W. J., Serreze, M. C., & Box, J. E. (2012) The role of albedo and accumulation in the 2010 melting record in Greenland. *Environmental Research Letters*, 6, 014005, doi:10.1088/1748-9326/6/1/014005

van As, D. (2011) Warming, glacier melt and surface energy budget from weather station observations in the Melville Bay region of northwest Greenland. *Journal of Glaciology*, 57, 208–220, doi: 10.3189/002214311796405898.

van de Wal, R. S. W., & Oerlemans, J. (1994) An energy balance model for the Greenland ice sheet. *Global Planetary Change*, 9, 115–131.

Van de Wal, R.S.W., Boot, W., Smeets, C.J.P.P., Snellen, H., van den Broeke, M.R., and Oerlemans, J. (2012) Twenty-one years of mass balance observations along the K-transect, west Greenland, *Earth System Science Data*, 4, 31–35, doi: 10.5194/essd-4-31-2012.

Van den Broeke, M. R., Smeets, C. J. P. P., Ettema, J., and Kuipers Munneke, P. (2008) Surface radiation balance in the ablation zone of the west Greenland ice sheet. *Journal of Geophysical Research – Atmosphere*, 113, D13105.

van den Broeke, M.R., Bamber, J., Ettema, J., Rignot, E., Schrama, E., van de Berg, W. J., van Meijgaard, E., Velicogna, I., & Wouters, B (2009) Partitioning recent Greenland mass loss, Science (New York, N.Y.), 326, 984–6, doi:10.1126/science.1178176, 200.

Vandecrux, B.R.M., Fausto, R.S., Langen, P.L., Van As, D., MacFerrin, M., Colgan, W.T., Ingeman-Nielsen, T., Steffen, K., Jensen, N.S., Møller, M.T. & Box, J.E. (in review) Drivers of Firn Densification on the Greenland Ice Sheet Revealed by Weather Station Observations and Modelling. *JGR: Earth Surface, in review*.

Vaughan, D.G., J.C. Comiso, I. Allison, J. Carrasco, G. Kaser, R. Kwok, P. Mote, T. Murray, F. Paul, J. Ren, E. Rignot, O. Solomina, K. Steffen and T. Zhang (2013) Observations: Cryosphere. In: Climate Change 2013: The Physical Science Basis. Contribution of Working Group I to the Fifth Assessment Report of the Intergovernmental Panel on Climate Change [Stocker, T.F., D. Qin, G.-K. Plattner, M. Tignor, S.K. Allen, J. Boschung, A. Nauels, Y. Xia, V. Bex and P.M. Midgley (eds.)]. Cambridge University Press, Cambridge, United Kingdom and New York, NY, USA

Vionnet, V., Brun, E., Morin, S., Boone, A., Faroux, S., Le Moigne, P., Martin, E. & Willemet, J.M. (2012) The detailed snowpack scheme Crocus and its implementation in SURFEX v7.2. *Geoscientific Model Development*, 5, 773–791. doi: 10.5194/gmd-5-773-2012

Wang, W., Zender, C.S., van As, D., Smeets, P.C.J.P., van den Broeke, M.R. (2016) A Retrospective, Iterative, Geometry-Based (RIGB) tilt-correction method for radiation observed by automatic weather stations on snow-covered surfaces -- application to Greenland. *The Cryosphere,* 10, 727-741.

Warren, S.G. (1982) Optical properties of snow. *Reviews of Geophysics and Space Physics,* 20, 1, 67-89.

Warren, S.G., and Wiscombe, W. (1980) A model for the spectral albedo of snow. II: Snow containing atmospheric aerosols, *Journal of Atmospheric Sciences,* 37, 2734–2745.

Wiscombe, W. J., and Warren, S. G. (1980) A model for the spectral albedo of snow. I: Pure snow, *Journal of Atmospheric Sciences*, 37, 2712–2733.

Winther, J. G. (1993), Short-term and long-term variability of snow albedo, Nordic Hydrology., 24, 199–212.

WSL (2018) Snow Metamorphism. [Accessed online at: https://www.slf.ch/en/snow/snow-as-a-substance/snow-metamorphism.html]

Zhuravleva, T.B. & Kokhanovsky, A.A. (2011) Influence of surface roughness on the reflective properties of snow. *Journal of Quantitative Spectroscopy and Radiative Transfer*, 112, 8, 1353-1368.